

On the relationship between mean observations, spatial averages and the Dyer-Roeder approximation in Einstein-Straus models

S. M. Koksang

Department of Physics, University of Helsinki and Helsinki Institute of Physics,
P.O. Box 64, FIN-00014 University of Helsinki, Finland

E-mail: sofie.koksang@helsinki.fi

Abstract. The redshift and redshift-distance relation in different Einstein-Straus models are considered. Specifically, the mean of these observables along 1000 light rays in different specific models are compared with predictions based on the Dyer-Roeder approximation and relations based on spatial averaging. It is shown that in certain limits, including those studied earlier in the literature, the Dyer-Roeder approximation and relations based on spatial averages agree with each other to a good precision regarding the redshift and redshift-distance relation and make good predictions of the mean of the exact relations. In limits where the two methods disagree, the Dyer-Roeder approximation clearly yields the better approximation of the true mean. This is explained by demonstrating the effect of boundary terms and integrated Sachs-Wolfe contributions but it is pointed out that the result seems to be valid for other Swiss-cheese models as well.

An expression for the redshift drift in Einstein-Straus models is presented and used for studying the behavior of this quantity in particular Einstein-Straus models.

Keywords: gravity, gravitational lensing, cosmic web, standard candles

Contents

1	Introduction	1
2	The Einstein-Straus model	4
3	Light propagation formalism for the Einstein-Straus model	6
3.1	Redshift drift in Einstein-Straus models	6
3.2	Numerical implementation	7
4	Mean observations in Einstein-Straus models	8
4.1	Redshift contributions	13
4.2	Redshift drift	19
4.3	Note on interior FLRW regions	21
5	Summary	22
6	Acknowledgments	22
A	Boundary contributions to expansion rate and shear	23

1 Introduction

The Universe is spatially inhomogeneous but we describe it and interpret observations with the spatially homogeneous Friedmann-Lemaître-Robertson-Walker (FLRW) models. This works remarkably well as seen in e.g. [1] (but is perhaps best illustrated by the precision required to identify the observational issues that standard cosmology is nonetheless facing - see e.g. [2–6]). While the observational issues with the Λ CDM model obviously lead to justified intrigue and raises important questions, an important issue is also raised by the good overall agreement between the FLRW model and observations made in a universe that is manifestly inhomogeneous, with observations based on light beams of different sizes and hence subjected to vastly different degrees of inhomogeneity. This issue is known as the fitting problem [7, 8].

The fitting problem can be summarized as the questions of how, why and to what extent observations can be described by a single FLRW model and how this ‘best fit’ FLRW model is related to the large scale geometry and dynamics of the Universe (this ‘best fit’ FLRW model will henceforth be referred to as the background). One approach to study the fitting problem is to consider how spacetime inhomogeneities affect observations. This has been done in a variety of ways including e.g. with perturbation theory (e.g. [9–18]) and other types of analytical arguments (e.g. [19–32]), using exact (e.g. [32–58]) and approximate (e.g. [59–63]) cosmological models, different types of stochastic models (e.g. [64, 65]), numerical relativity (e.g. [66, 67]) and Newtonian (e.g. [68–70]) and relativistic [71] N-body simulations. The question has also been studied in light of cosmic backreaction [72, 73], in terms of how to describe mean observations in a universe with non-negligible cosmic backreaction (e.g. [74–76]) and in the timescape scenario [77–82]. A recent review on the topic of small-scale inhomogeneities’ effect on observations is given in [83].

One of the most well-known outcomes of the studies of how inhomogeneities affect observations is the Dyer-Roeder approximation [24, 25] (see also [26]). The Dyer-Roeder approximation is a redshift-distance relation which has been modified compared to the ordinary FLRW relation in an attempt to take into account the overall effect it has on the redshift-distance relation that thin beams of light (e.g. from supernovae) probe the Universe at scales so small that the corresponding matter distribution is best modeled (mainly) as opaque clumps. The approximation amounts to assuming that the redshift is unaffected by the inhomogeneities and hence is described according to the background FLRW model, while the angular diameter distance is approximated by neglecting the Weyl focusing and adjusting the Ricci focusing with a constant, α . The resulting expression is ($c = 1$ throughout)

$$\frac{d^2 D_A}{dz^2} + \left(\frac{2}{1+z} + \frac{d \ln H}{dz} \right) \frac{d D_A}{dz} = - \frac{4\pi G \rho}{H^2 (1+z)^2} \alpha D_A, \quad (1.1)$$

where z is the redshift given according to the background FLRW model.

The Dyer-Roeder expression has been modified in several works, e.g. with focus on a possible redshift dependence of α [30, 64, 84]. This highlights the unfortunate detail that the value of α is not *a priori* predicted by the Dyer-Roeder approximation and must therefore either be considered a new model parameter or somehow estimated.

The Dyer-Roeder approximation has been critiqued by several different authors. Critique has, for instance, been based on asserting that it is inconsistent to modify the mean density along the light ray without also modifying the expansion rate [29, 85, 86], including when computing the redshift¹ (see also references in [29]). In addition, some studies show a disagreement with the Dyer-Roeder approximation. One interesting line of study which appears to not generally agree with the Dyer-Roeder approximation is that which is based on attempting to relate observations to spatial averages [27, 28, 31]. Specifically, in [27, 28] it was assessed that if spacetime admits a foliation of spatial hypersurfaces of statistical homogeneity and isotropy with inhomogeneities evolving slowly compared to the time it takes a light ray to traverse the assumed homogeneity scale, then the redshift and angular diameter distance can be computed using spatially averaged quantities according to

$$\frac{d^2 D_A}{dz_{\text{av}}^2} + \left(\frac{2}{1+z_{\text{av}}} + \frac{d \ln H_{\text{av}}}{dz_{\text{av}}} \right) \frac{d D_A}{dz_{\text{av}}} = - \frac{4\pi G \rho_{\text{av}}}{H_{\text{av}}^2 (1+z_{\text{av}})^2} D_A, \quad (1.2)$$

where ρ_{av} is the smooth density obtained by averaging on some spatial domain above the homogeneity scale, and H_{av} is similarly a third of the averaged local expansion rate θ . The redshift is here given by

$$1 + z_{\text{av}} = \exp \left(\int_{t_e}^{t_0} dt H_{\text{av}} \right), \quad (1.3)$$

where t_0 is the time of observation and t_e that of emission. The spatial average of a scalar S is defined as $S_{\text{av}} := \frac{\int_D S dV}{\int_D dV} =: \langle S \rangle$, where dV is the proper infinitesimal volume element of

¹As in chapter 4 of [87] one may note that multiplying ρ by a constant factor leaves the fluid expansion rate unchanged according to the mass conservation law for dust. In [87], this is given as an argument for keeping the expansion rate fixed to that of the background in the Dyer-Roeder approximation. However, such argument seems to go beyond the original Dyer-Roeder approximation which solely addresses the question of mean observational relations and it is not clear how such mean observations can be combined with (local or average) dynamical equations - indeed, understanding how to do this is an essential part of the fitting problem.

the spatial hypersurfaces and D is a spatial domain larger than the homogeneity scale.

Equations 1.2 and 1.3 are based on the assumption that the content of the Universe can be described as dust that is comoving according to the foliation with statistically homogeneous and isotropic spatial hypersurfaces. The equations were generalized in [28] but this generalization will not be needed here.

The predicted relations in equations 1.2 and 1.3 will in the following be referred to as the “relations based on spatial averages”.

Both the Dyer-Roeder approximation and the relations based on spatial averages are meant to describe the redshift-distance relation in a mean sense, i.e. after averaging over a large number of light rays so that fluctuations along the individual light rays due to local inhomogeneities can be neglected. While the Dyer-Roeder approximation explicitly assumes that there are opaque regions that light rays cannot sample, the relations based on spatial averages were derived assuming that light rays trace spacetime “fairly” i.e. that there are no opaque regions. A naive extension of the analyses in [27, 28] to include opaque regions would, however, imply that the averages in equations 1.2 and 1.3 should simply only include the regions that light rays are permitted to travel through. One then sees that this naive extension and the Dyer-Roeder approximation do not agree since the Dyer-Roeder approximation misses the effect inhomogeneities have on the redshift.

The Dyer-Roeder approximation is largely an assumption and e.g. does not provide a recipe for computing α , making it somewhat less useful for making predictions. On the other hand, the method based on spatial averages is based on a thorough, detailed analysis which, to this author’s knowledge, has not been critiqued. It is therefore intriguing that a study based on an exact solution to the Einstein equations (Einstein-Straus models [88]) showed that for the studied class of cosmological solutions, the Dyer-Roeder approximation is actually correct [32]. The study did not include much consideration of spatial averages so it did not pinpoint why the analyses of [27, 28] as well as the earlier work in e.g. [31] seems to fail for spacetimes with opaque regions.

The literature does not yet contain clear and hence satisfying answers to the questions collectively going under the name the fitting problem. Obtaining these answers is vital for fully understanding e.g. the significance of parameter determinations obtained when interpreting observations with FLRW models, including possible biases which, if not taken into account, could lead to e.g. wrong determinations of global energy densities, curvature and expansion rate. The goal with the study presented here is therefore to supplement the study in [32] by considering light propagation in Einstein-Straus models from the perspective of spatial averages, in order to obtain a better understanding of under what circumstances the two redshift-distance relations in equations 1.1 and 1.2 are applicable.

While the redshift and redshift-distance relation are important for interpreting many well-known observables such as CMB, supernovae and BAO observations, future astrophysical surveys will include new types of observables. One such example is the redshift drift, Δz , which describes how the observed redshift of a given comoving source is seen to change with time (according to a comoving observer). In an FLRW universe, the redshift drift in a time interval Δt_0 is given by

$$\Delta z = \Delta t_0(1+z)(a_{,t}(t_0) - a_{,t}(t_e)), \quad (1.4)$$

i.e. the redshift drift is non-vanishing if the expansion rate of the Universe changes with time and its sign depends on whether the expansion accelerates or decelerates between the times of observation and emission.

In an inhomogeneous universe, the expression for the redshift drift is necessarily more complicated. The expression has been identified in spherically symmetric models with an observer placed in the center of symmetry [89], Lemaitre-Tolman-Bondi models [90], Szekeres models [91–93], Stephani models [94] and Bianchi I models [95]. A fairly simple expression for the redshift drift in a general spacetime can be obtained quite easily by using the exact definition, $\Delta z := \frac{dz}{dt_0} \Delta t_0$, at least for the case of comoving source and observer. This is shown in [96] where it is also shown by explicit examples that the mean redshift drift in inhomogeneous cosmological models may deviate from the drift of the mean redshift (in agreement with the results in [97]). The method presented in [96] will here be used to study the redshift drift in Einstein-Straus models.

In section 2 below, the Einstein-Straus models will be introduced. Section 3 describes how light propagation can be described in the models. Numerical results and analytical investigations of the (mean) redshift, redshift-distance relation and redshift drift are presented in section 4 and a summary with concluding remarks is given in section 5.

2 The Einstein-Straus model

Inhomogeneous cosmological models can be constructed as so-called Swiss-cheese models where spatially spherical regions of an FLRW spacetime are replaced by other solutions to the Einstein equations. The Einstein-Straus model was introduced in [88] as the first ever Swiss-cheese model constructed by replacing spatially spherically symmetric patches of an Einstein-de Sitter (EdS) spacetime with spherically symmetric exterior Schwarzschild patches. Light propagation was studied in these models already in 1969 in [34] and was recently revisited in [32, 33] where the model was extended to include a cosmological constant.

The Swiss-cheese model studied here is similar to the original Einstein-Straus model so the line element of the cheese (the FLRW “background”) is that of the EdS model, i.e.

$$ds^{\text{cheese}} = -dT^2 + a^2 (d\xi^2 + \xi^2 d\Omega^2), \quad (2.1)$$

where $a = \left(\frac{T}{T_0}\right)^{2/3}$ is the scale factor normalized to 1 at present time, $T = T_0$.

The line element of the Schwarzschild “holes” is given by

$$ds^{\text{hole}} = -A(r)dt^2 + B(r)dr^2 + r^2 d\Omega^2. \quad (2.2)$$

For the exterior Schwarzschild solution, the metric functions A and B are given by $A = 1 - \frac{2M}{r}$, $B = \left(1 - \frac{2M}{r}\right)^{-1}$, where M is the effective gravitational mass of the central/interior part of the Schwarzschild spacetime. The exterior Schwarzschild metric represents the vacuum outside a spherically symmetric massive body and it can be combined with other spacetimes representing this interior massive region. The interior region can for instance be another FLRW model or a spherically symmetric Stephani solution [98] but the simplest interior region is given by the interior Schwarzschild solution. In this case, the metric functions are

given by

$$A(r) = \begin{cases} \frac{1}{4} \left(3\sqrt{1 - \frac{2M}{r_{\text{bie}}}} - \sqrt{1 - \frac{2Mr^2}{r_{\text{bie}}^3}} \right)^2 & \text{if } r < r_{\text{bie}} \\ 1 - \frac{2M}{r} & \text{otherwise} \end{cases} \quad (2.3)$$

and

$$B(r) = \begin{cases} \left(1 - \frac{2Mr^2}{r_{\text{bie}}^3} \right)^{-1} & \text{if } r < r_{\text{bie}} \\ \left(1 - \frac{2M}{r} \right)^{-1} & \text{otherwise} \end{cases}, \quad (2.4)$$

where r_{bie} denotes the value of r on the boundary between the interior and exterior Schwarzschild metric. An interior Schwarzschild solution is usually not considered in cosmological contexts because it describes a perfect fluid with a (in general) non-physical equation of state parameter. However, the principles of light propagation do not depend on equation of state parameters being physically reasonable. Hence, the interior Schwarzschild region may be used for studying the principles of light propagation in situations where an interior region is desired. Minor results will therefore be presented based on including the interior Schwarzschild regions in the Einstein-Straus model.

The interior Schwarzschild solution has a constant density related to M by $\rho_{\text{interior}} = \frac{M}{\frac{4}{3}\pi r_{\text{bie}}^3}$ and an r -dependent pressure [99]

$$p = \rho \frac{\sqrt{1 - \frac{2Mr^2}{r_{\text{bie}}^3}} - \sqrt{1 - \frac{2M}{r_{\text{bie}}}}}{3\sqrt{1 - \frac{2M}{r_{\text{bie}}}} - \sqrt{1 - \frac{2Mr^2}{r_{\text{bie}}^3}}}. \quad (2.5)$$

This form of the pressure is determined by requiring that the pressure vanishes on the boundary between the interior and exterior Schwarzschild regions. For the models studied here, the pressure is subdominant to the density to the extent that it is negligible for the precision needed here.

In order to be an exact solution to the Einstein equations, a Swiss-cheese model must fulfill the Darmois junction conditions [100] which require the extrinsic curvature as well as the metric on the boundary between different solutions to be continuous. The Darmois junction conditions for the Einstein-Straus model are well known (see e.g. [33, 101]) and are

$$r_{\text{b}} = a\xi_{\text{b}}, \quad (2.6)$$

where $r_{\text{b}}, \xi_{\text{b}}$ are the values of r, ξ at the junction of the two spacetimes, and

$$M = \frac{4\pi G\rho_0}{3}\xi_{\text{b}}^3, \quad (2.7)$$

where G is Newton's constant and ρ_0 is the present time energy density in the EdS model. For a given M , ξ_{b} (and hence r_{b}) is uniquely determined. On the other hand, r_{bie} can be chosen freely, though keeping in mind that $\frac{GM}{r_{\text{bie}}} < \frac{4}{9}$ is required to avoid infinite pressure [99], and that the model can only be considered for time intervals where $r_{\text{bie}} < r_{\text{b}} = r_{\text{b}}(t)$.

Models with three different sets of parameter values will be considered here, with model parameters specified in section 3.2

3 Light propagation formalism for the Einstein-Straus model

The straightforward way to study light propagation in an Einstein-Straus model is to use the null-geodesic equations

$$\frac{d}{d\lambda} (g_{\alpha\beta} k^\beta) = \frac{1}{2} g_{\mu\nu, \alpha} k^\mu k^\nu \quad (3.1)$$

and the transport equation (see e.g. [102])

$$\frac{d^2 D_b^a}{d\lambda^2} = T_c^a D_b^c, \quad (3.2)$$

where λ is an affine parameter along the null geodesic and T_c^a is the tidal matrix which can be written as

$$T_{ab} = \begin{pmatrix} \mathbf{R} - \text{Re}(\mathbf{F}) & \text{Im}(\mathbf{F}) \\ \text{Im}(\mathbf{F}) & \mathbf{R} + \text{Re}(\mathbf{F}) \end{pmatrix}, \quad (3.3)$$

where $\mathbf{R} := -\frac{1}{2} R_{\mu\nu} k^\mu k^\nu$ and $\mathbf{F} := -\frac{1}{2} R_{\alpha\beta\mu\nu} (\epsilon^*)^\alpha k^\beta (\epsilon^*)^\mu k^\nu$. $R_{\alpha\beta\mu\nu}$ is the Riemann tensor and $\epsilon^\mu := E_1^\mu + iE_2^\mu$ is a complex combination of two orthogonal vectors spanning the space orthogonal to both k^μ and u^μ . E_1^μ and E_2^μ must fulfill certain orthonormality conditions, namely $E_i^\mu E_\mu^j = \delta_j^i$, $E_i^\mu u_\mu = 0 = E_i^\mu k_\mu$, $i, j \in 1, 2$. E_1^μ and E_2^μ are typically parallel propagated along the light rays with initial conditions fulfilling these requirements. When the (comoving) observer is placed in the FLRW cheese, initial conditions can be chosen as

$$E_1^\mu \propto \left(0, \xi^2 \left((k^\theta)^2 + \sin^2(\theta) (k^\phi)^2 \right), -k^r k^\theta, -k^r k^\phi \right) \quad (3.4)$$

$$E_2^\mu \propto \left(0, 0, k^\phi, \frac{-k^\theta}{\sin^2(\theta)} \right). \quad (3.5)$$

The Weyl tensor vanishes in the EdS region so $k^\mu k_\mu = 0$ implies that $\mathbf{F} = 0$ there. The exterior Schwarzschild region is a vacuum spacetime so $\mathbf{R} = 0$ but $\mathbf{F} \neq 0$. In the interior Schwarzschild spacetime region, both \mathbf{F} and \mathbf{R} are non-vanishing.

The angular diameter distance is given by $D_A = \sqrt{|\det D|}$. Therefore, the transport equation is solved simultaneously with the geodesic equations in order to obtain the exact redshift-distance relation along individual light rays.

3.1 Redshift drift in Einstein-Straus models

The redshift drift in Einstein-Straus models can be computed following the procedure presented in [96], i.e. by differentiating $1+z = \frac{(u^\alpha k_\alpha)_e}{(u^\beta k_\beta)_0}$ with respect to observer present time. The expression depends on the position of observer and emitter. Here, the redshift drift will only be computed with both observer and emitter in the FLRW region. In this case, the expression for the redshift drift is

$$\begin{aligned} \frac{\Delta z}{\Delta T_0} &= -\frac{(1+z)}{k_0^T} \frac{\partial k^T}{\partial T} \Big|_0 + \frac{1}{k_0^T} \frac{1}{1+z} \frac{\partial k^T}{\partial T} \Big|_e \\ &= -\frac{(1+z)}{(k_0^T)^2} \left(\frac{dk^T}{d\lambda} - k^i k_{,i}^T \right) \Big|_0 + \frac{1}{k_e^T k_0^T} \frac{1}{1+z} \left(\frac{dk^T}{d\lambda} - k^i k_{,i}^T \right) \Big|_e. \end{aligned} \quad (3.6)$$

In the limit where the light ray only travels in the EdS region, $k^T = \frac{-1}{a}$ and $k_{,T}^T = \frac{1}{k^T} \frac{dk^T}{d\lambda}$, and the above expression reduces to the ordinary FLRW expression $\Delta z = \Delta T_0 (H_0(1+z) - H_e)$

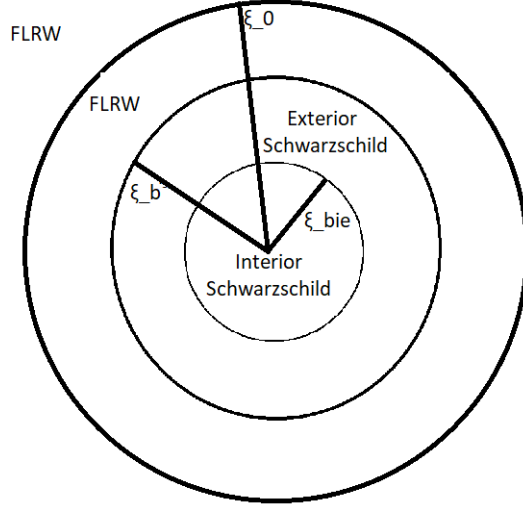


Figure 1. Sketch of Swiss-cheese setup illustrating the relationship between ξ_0 , ξ_{bie} and ξ_b . The coordinate $\xi_{\text{bie}} := ar_{\text{bie}}$ is defined analogously to $a\xi_b = r_b$.

as it should. However, in the Einstein-Straus model, $\frac{dk^T}{d\lambda} := k^\alpha k_{,\alpha}^T$ will not necessarily reduce simply to $k^T k_{,T}^T$ along the entire light ray. The redshift drift may therefore differ from Δz_{EdS} if the particular light ray traverses one or more Schwarzschild regions.

In order to compute the redshift drift, $k_{,T}^T := \frac{\partial k^T}{\partial T}$ must be computed along the light rays. This is achieved by solving the equations $\frac{dk_{,\nu}^\mu}{d\lambda}$ simultaneously with the geodesic equations and the transport equations. The expressions for $\frac{dk_{,\nu}^\mu}{d\lambda}$ are found from the relation [40]

$$\frac{d}{d\lambda} k_{,\nu}^\mu = \frac{\partial}{\partial x^\nu} \frac{dk^\mu}{d\lambda} - k_{,\nu}^\beta k_{,\beta}^\mu. \quad (3.7)$$

Since the observer is placed in the FLRW region, initial conditions can be set according to a spatially homogeneous universe where $k_{,x}^\mu = k_{,y}^\mu = k_{,z}^\mu = 0$ (which becomes somewhat more complicated when transforming to spherical coordinates which were used here).

Before moving on, note that the drift of z_{av} is given by a formula similar to that of FLRW models, namely as $\Delta z_{\text{av}} = \Delta T_0 ((1 + z_{\text{av}}) H_{0,\text{av}} - H_{\text{av}})$ (see e.g. [103]).

3.2 Numerical implementation

The redshift-distance relation is computed by assembling the Einstein-Straus models on-the-fly, i.e. along the given light ray during its propagation. In practice, each light ray has been initialized in the EdS background at a fixed comoving value of ξ , $\xi = \xi_0$ (the value of ξ_0 for each studied model is given in table 1). The initial values of k^r , k^θ and k^ϕ are random, though with $k^r \leq 0$ and such that the null condition is fulfilled with the initial condition $k^T = -\frac{1}{c}$. When a light ray again reaches $\xi = \xi_0$, it is turned back towards the Schwarzschild structure with a new random impact parameter. If the inner Schwarzschild region is considered opaque, a light ray reaching $r \leq r_{\text{bie}}$ is moved back to the previous time it reached $\xi = \xi_0$ and turned back towards the Schwarzschild structure with new (random) impact parameter.

Model name	M (M_\odot)	r_{bie} (Mpc)	ξ_b (Mpc)	ξ_0 (Mpc)
model 1	10^{15}	1	12.06	12.3
model 2	10^{16}	10	25.99	26.1
model 3	10^{16}	10	25.99	28.5

Table 1. Model parameters of the studied Einstein-Straus models.

A sketch of the setup with boundaries at three radial coordinate values is shown in figure 1. Three different models will be considered, with parameter values given in table 1.

At the boundary between the EdS and Schwarzschild region, a coordinate transformation is necessary. Specifically, (T, ξ) are transformed into (t, r) and the null-vector and screen space basis vectors are also transformed accordingly. The transformation rules were given in [33] and are here re-stated for convenience:

$$\frac{dT}{dt} = A \quad (3.8)$$

$$r = a\xi \quad (3.9)$$

$$k^r = ak^\xi + \sqrt{1 - Ak^T} \quad (3.10)$$

$$k^t = \frac{1}{A}k^T + \frac{a}{A}\sqrt{1 - Ak^\xi}, \quad (3.11)$$

(Note that for the particular models studied here, $|A(r_b(T)) - 1| < 10^{-4}$ so setting $t = T$ on the boundary is a reasonable approximation.)

The partial differentials of the FLRW and Schwarzschild coordinates ($\frac{\partial T}{\partial r}$ etc.) can be seen by comparing equations 3.10 and 3.11 with the general formula for coordinate transformations of 4-vectors, $k^{\mu'} = \frac{\partial x^{\mu'}}{\partial x^\nu} k^\nu$. These can then be used to transform covariant derivatives of k^μ between the two coordinate systems according to $k_{;\nu'}^{\mu'} = \frac{\partial x^{\mu'}}{\partial x^\mu} \frac{\partial x^\nu}{\partial x^{\nu'}} k_{;\nu}^\mu$ and from these, the partial derivatives, $k_{;\nu}^\mu = k_{;\nu}^\mu - \Gamma_{\nu\gamma}^\mu k^\gamma$, can be computed when going between FLRW and Schwarzschild regions.

4 Mean observations in Einstein-Straus models

This section presents the results from propagating 1000 light rays out to $z = 1$ in different Einstein-Straus models and compares the results to the Dyer-Roeder approximation and the relations based on spatial averages. An individual light ray may be in either region type (Schwarzschild or EdS) when it reaches $z = 1$ but all light rays are initialized in the EdS region at $\xi = \xi_0$, i.e. the observer is always placed in the EdS region at $\xi = \xi_0$.

Figure 2 shows the mean and dispersion of the redshift-distance relation in model 1 which has $M = 10^{15} M_\odot$ and $r_{\text{bie}} = 1 \text{Mpc}$, the inner Schwarzschild region ($r < r_{\text{bie}}$) being opaque. The observer was placed in the FLRW region at $\xi_0 = 12.3 \text{Mpc}$. This situation resembles those studied in [32, 33]. As in [32, 33], it is seen that the Dyer-Roeder approximation overestimates the actual mean redshift-distance relation somewhat. As explained in [32], this is

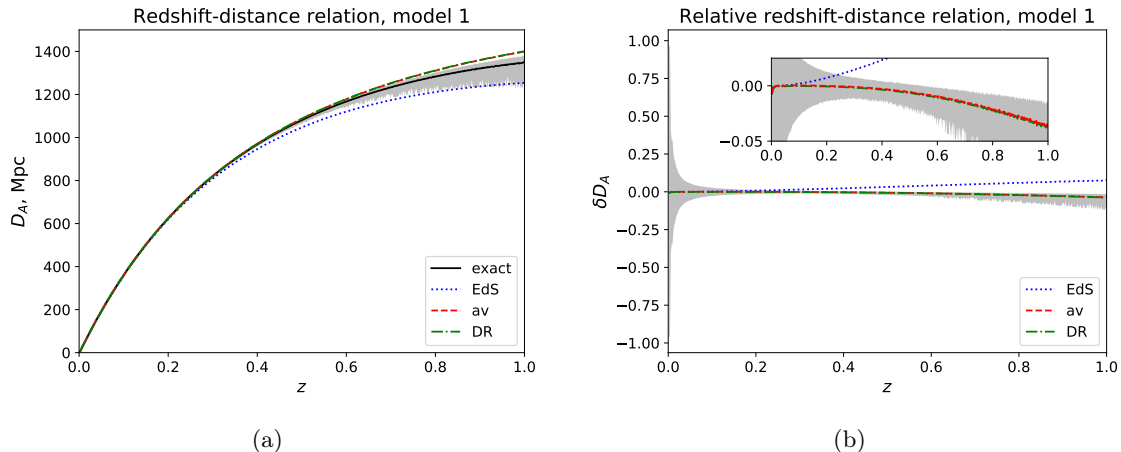


Figure 2. Mean angular diameter distance along 1000 light rays in model 1. The figure to the left shows D_A while the figure to the right shows $\delta D_A := \frac{D_A - \bar{D}_A}{D_A}$, where D_A is the exact angular diameter distance along the light rays and \bar{D}_A is the angular diameter distance according to either the EdS model, the expression based on the spatial averaging scheme (“av”) or the Dyer-Roeder approximation (“DR”). The gray shaded area shows the dispersion around the mean. In the figure to the right, the dispersion is shown for $\frac{D_A - D_{A,DR}}{D_{A,DR}}$.

due to shear which is neglected in the Dyer-Roeder approximation and as shown in [65] it can partially be corrected for.

In [32], it was asserted that spatial averaging is nonsensical in an Einstein-Straus model because there is no natural way to define a 3+1 foliation in the vacuum regions. The parameter α for the Dyer-Roeder approximation was estimated by the fraction of time the light rays spent in the Schwarzschild versus FLRW spacetime regions. Here, it is instead claimed that spatial averaging makes perfect sense in Einstein-Straus models despite there being vacuum regions; the redshift-distance relation of [27], reiterated in equations 1.2 and 1.3 in the introduction, was specifically derived for averages computed on spatial hypersurfaces of statistical homogeneity and isotropy. It is therefore the distribution of structures that determines the “natural” 3+1 foliation for spatial averaging, also in the Einstein-Straus model where there are vacuum regions. Since the Einstein-Straus models studied here are based on distributing Schwarzschild holes randomly in an FLRW cheese, it is the hypersurfaces of constant T which represent the hypersurfaces of statistical homogeneity and isotropy and hence the hypersurfaces on which the spatial averages should be computed.

Figure 2 serves to explicitly show that, in fact, the Dyer-Roeder approximation and the relation based on spatial averages give the same prediction for the behavior of the mean redshift-distance relation for this particular model - and it also does so in the models studied in [32, 33]. To understand why the two procedures give the same prediction, it is necessary to compute the spatially averaged quantities on the spatially spherical region corresponding to $\xi \leq \xi_0$, excluding the opaque region at the center. To do this, first note that the deviation of A from unity is sub-percent for at least $0.1 \lesssim r$, so the hypersurfaces of $t = \text{const.}$ make a good approximation to the hypersurfaces corresponding to $T = \text{const.}$. Therefore, the spatial averages on the relevant region ($\xi \leq \xi_0$, $r \geq r_{\text{bie}}$) are the spatial averages on the surface with constant T in the region $\xi_b \leq \xi \leq \xi_0$ plus the spatial averages on the surface with constant t in the region $r_{\text{bie}} \leq r \leq r_b$. The deviations of B from 1 is sub-percent as well, so this is also

set to 1 when computing spatial averages. Lastly, since sub-percent accuracy is not of interest in this study, the volume of the opaque inner region may be neglected because it makes up such a small fraction of the entire relevant spatial volume.

The relevant spatially averaged quantities are now straight forward to compute and are

$$\langle \rho \rangle = \frac{\int_{\xi_b}^{\xi_0} \xi^2 d\xi \rho_{\text{EdS}}}{\frac{1}{3}\xi_0^3} = \frac{\rho_{\text{EdS}} (\xi_0^3 - \xi_b^3)}{\xi_0^3} := \alpha \rho_{\text{EdS}} \quad (4.1)$$

$$\langle \theta \rangle = \frac{3H_{\text{EdS}} (\xi_0^3 - \xi_b^3)}{\xi_0^3} + \langle \theta_b \rangle. \quad (4.2)$$

In the computations, it was utilized that the Schwarzschild metric is stationary so has $\theta = 0$, while $\theta = 3H_{\text{EdS}}$ in the EdS region.

Equation 4.1 gives the prediction for the Dyer-Roeder parameter α used when computing the Dyer-Roeder approximated redshift-distance relation for figure 2, namely $\alpha = \frac{\xi_0^3 - \xi_b^3}{\xi_0^3}$. Equation 4.2 highlights that in order to compute the average expansion rate determining z_{av} (see equation 1.3), the contribution from the boundary expansion rate, θ_b , must be obtained. This boundary term appears because the velocity field of comoving observers changes abruptly on the boundary between the Schwarzschild and EdS regions. As shown in appendix A, such finite jumps can be modeled through a Heaviside function which upon taking a derivative (to go to the expansion rate) becomes a delta function, indicating that the boundary itself must be attributed an expansion rate. The value of the boundary expansion rate can be estimated by considering a Lemaitre-Tolman-Bondi (LTB) model [104–106] which for $\xi > \xi_b$ expands as an EdS model while being static for $\xi < \xi_b$. This estimate is computed in appendix A where it is found to be

$$\theta_b = \xi \delta(\xi - \xi_b) H_{\text{EdS}}, \quad (4.3)$$

where $\delta(\xi - \xi_b)$ is the delta function centered at $\xi = \xi_b$.

Inserting this estimate for θ_b into equation 4.2 yields

$$\begin{aligned} \langle \theta \rangle &= \frac{(\xi_0^3 - \xi_b^3) H_{\text{EdS}} + \int_0^{\xi_0} d\xi H_{\text{EdS}} \delta(\xi - \xi_b) \xi^3}{\frac{1}{3}\xi_0^3} \\ &= \frac{(\xi_0^3 - \xi_b^3) H_{\text{EdS}} + \xi_b^3 H_{\text{EdS}}}{\frac{1}{3}\xi_0^3} = 3H_{\text{EdS}}. \end{aligned} \quad (4.4)$$

Thus, the volume averaged expansion rate on surfaces of statistical homogeneity and isotropy is that of the EdS model². This implies that the naive extension of the analyses of [27, 28, 31] to include opaque regions predicts that, to a good approximation and for this particular setup, the mean redshift-distance relation is the same as in the Dyer-Roeder approximation with the equation for D_A modified by $\alpha = \frac{\xi_0^3 - \xi_b^3}{\xi_0^3}$ and the redshift given according to the background.

²Note that this result must be insensitive to the exact foliation used in the Schwarzschild region as long as the spatial hypersurfaces only deviate little from the $t = \text{const.}$ hypersurfaces. It is possible that hypersurface foliations fulfilling this requirement as well as having a smooth expansion rate across the boundary between the Schwarzschild and FLRW regions exist, whereby the result can be obtained without introducing a boundary contribution, θ_b . This e.g. seems to be the case for the hypersurfaces orthogonal to the free-falling velocity fields discussed in [32].

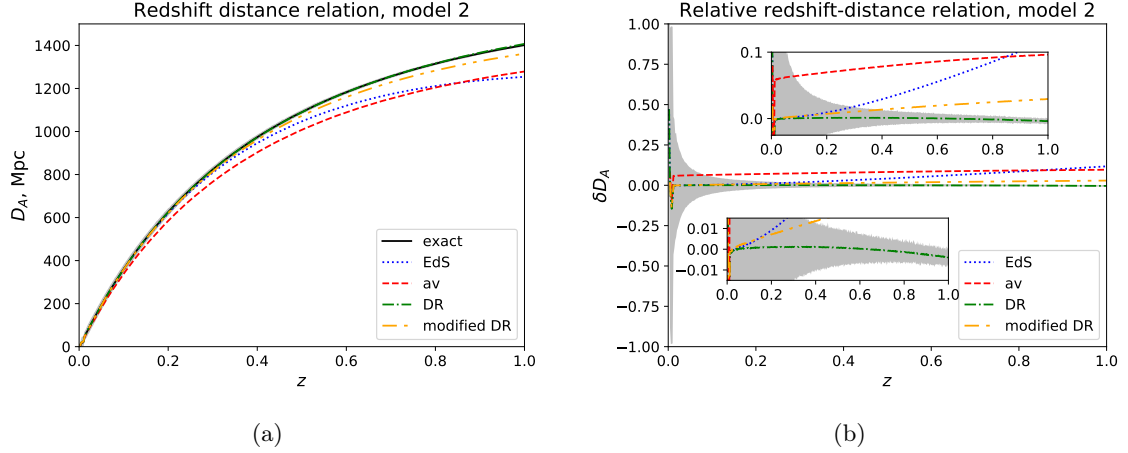


Figure 3. Mean angular diameter distance along 1000 light rays in model 2. The figure to the left shows D_A while the figure to the right shows $\delta D_A := \frac{D_A - \bar{D}_A}{D_A}$, where D_A is the exact angular diameter distance along the light rays and \bar{D}_A is the angular diameter distance according to either the EdS model, the expression based on the spatial averaging scheme (“av”), the Dyer-Roeder approximation (“DR”) or a modified Dyer-Roeder scheme (“modified DR”). A shaded area is included in the figure to the right to show the dispersion around the mean when \bar{D}_A is given according to the Dyer-Roeder approximation. A dispersion is not included in the figure to the left as it would not be discernible. Close-ups are shown in the figure to the right.

The results presented above show that the Dyer-Roeder approximation and the competing results based on spatial averages actually agree in the cases studied above and in [32, 33]. These setups are therefore ill-suited for distinguishing between the two approaches with explicit examples. In order to distinguish between the two approaches, a model that leaves $\langle \theta \rangle \not\approx 3H_{\text{EdS}}$ must be considered. This is easily achieved by extending the opaque, interior Schwarzschild region. For concreteness, an Einstein-Straus model with $r_{\text{bie}} = 10\text{Mpc}$, $\xi_0 = 26.1\text{Mpc}$ and $M = 10^{16}M_\odot$ has been studied (model 2). The large mass is introduced in order to exaggerate the effects of the inhomogeneities. The spatial averages must now be computed using the more accurate formulas (still neglecting the deviations of A, B from 1)

$$\langle \rho \rangle = \rho_{\text{EdS}} \frac{\xi_0^3 - \xi_{\text{b}}^3}{\xi_0^3 - \xi_{\text{bie}}^3} := \alpha \rho_{\text{EdS}} \quad (4.5)$$

$$\langle \theta \rangle = 3H_{\text{EdS}} \frac{\xi_0^3}{\xi_0^3 - \xi_{\text{bie}}^3}, \quad (4.6)$$

where $\xi_{\text{bie}} := r_{\text{bie}}/a$.

This time, the average expansion rate is significantly different from the EdS expansion rate and hence the volume averaged scale factor and corresponding redshift will deviate from the EdS redshift. The prediction of the spatially averaged redshift-distance relation therefore differs from that of the Dyer-Roeder approximation. This is seen in figure 3 where the mean and dispersion of the redshift-distance relation along 1000 light rays in model 2 are shown. As seen, the Dyer-Roeder approximation makes a good approximation of the mean redshift-distance relation while the predictions based on spatially averaged quantities are

Model	α
1	~ 0.06
2	$\sim 0.01 - 0.02$
3	$\sim 0.25 - 0.33$

Table 2. Value of α in mean-redshift interval $z \in [0, 1]$ for the studied models. Values are approximate as indicated by “ \sim ”.

clearly wrong. Following critique given of the Dyer-Roeder approximation in e.g. [29, 86], a mix between the Dyer-Roeder approximation and the method based on spatial averages, where all quantities in the equation for the angular diameter distance are the spatial averages while the redshift is the EdS redshift, is also included. This ‘modified Dyer-Roeder approximation’ does a poorer job than the ordinary Dyer-Roeder approximation does.

Note now that in both the models studied so far, α has been quite small. This means that the mean redshift-distance relations in models 1 and 2 are nearly those of empty beams. It is instructive to also look at a model which has a somewhat larger α . For this purpose, model 3 is constructed using the same parameters as model 2 except that it includes a larger FLRW volume. α for all three models is shown in table 2. Note that α varies in time because ξ_{bie} does.

Figure 4 shows the redshift-distance relation for model 3. The Dyer-Roeder approximation clearly still gives a much better approximation of the actual mean redshift-distance relation than the relations based on spatial averages and is also still better than the modified Dyer-Roeder approximation (though only barely). However, the difference between the Dyer-Roeder approximation and the actual mean redshift-distance relation is more significant than it was for models 1 and 2. This indicates that the spatial average used for computing α does not exactly capture the spacetime felt by the light rays on average; any such imprecision in averages will for the Dyer-Roeder approximation only affect α and hence does not have much impact when α is close to zero but will become visible when α becomes of order 0.1 – 1.

It is not surprising that the spatial averages do not coincide *exactly* with the “mean” spacetime felt by the light rays. First of all, the spatial averages on hypersurfaces of statistical homogeneity and isotropy can only in the case of a stationary metric be expected to correspond exactly to the mean felt by light rays. Second of all, as already discussed, the hypersurfaces used here for computing spatial averages and hence α are only approximately those of spatial homogeneity and isotropy. Lastly, while it is only the spherical regions for which $r \leq r_{\text{bie}}$ which are modeled as opaque, these opaque spheres effectively block an entire cone of the spacetime $\xi \leq \xi_0$ which a light ray cannot traverse. The correct volume averages must therefore be modified compared to those used above where only the spherical regions were considered opaque. However, the good agreement between the Dyer-Roeder approximation and mean redshift-distance relation in model 3 indicates that the spatial averages used here constitute quite good approximations of the average spacetime probed by the light rays.

Since the redshift is the quantity which most clearly differs between the Dyer-Roeder approximation and the relations based on spatial averages, it is instructive to look at the redshift in more detail. This is done in the following subsection.

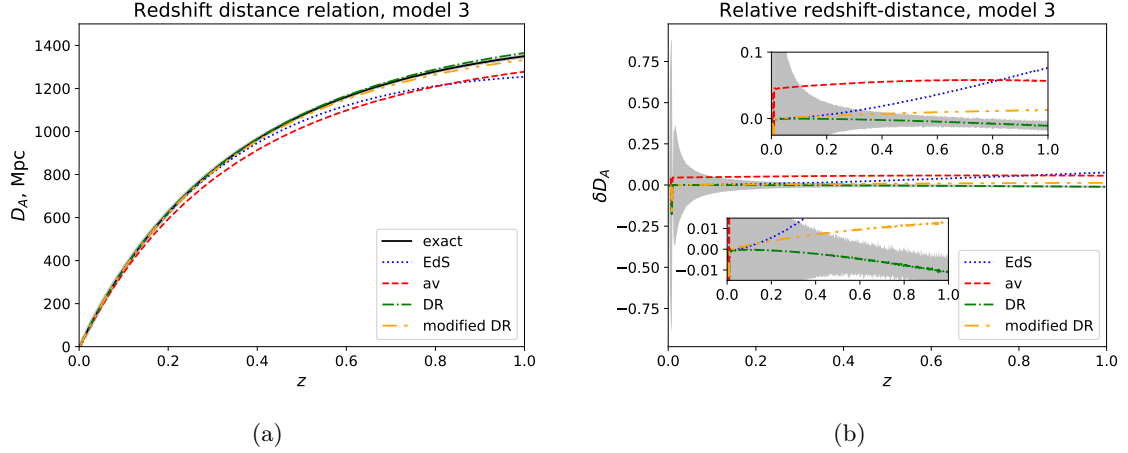


Figure 4. Mean angular diameter distance along 1000 light rays in model 3. The figure to the left shows D_A while the figure to the right shows $\delta D_A := \frac{D_A - \bar{D}_A}{D_A}$, where D_A is the exact angular diameter distance along the light rays and \bar{D}_A is the angular diameter distance according to either the EdS model, the expression based on the spatial averaging scheme (“av”), the Dyer-Roeder approximation (“DR”) or a modified Dyer-Roeder scheme (“modified DR”). A shaded area is included in the figure to the right to show the dispersion around the mean when \bar{D}_A is given according to the Dyer-Roeder approximation. A dispersion is not included in the figure to the left as it would not be discernible. Close-ups are shown in the figure to the right.

4.1 Redshift contributions

Figure 5 shows the mean of the deviation in the redshift compared to the EdS redshift for models 1, 2 and 3. As seen, in all three cases, the deviations from the EdS redshift are only around 0.2 % for $z \approx 1$, so the mean redshift is in all the studied cases very well approximated by the background redshift, z_{EdS} . One may however note that there seems to be an offset in the mean redshifts compared to the EdS redshift. This offset is clearest in models 2 and 3. It has been verified that this result is not a statistical fluke by computing the redshift along several different sets of 1000 random light rays. The offset seems to be robust. The origin of this offset has not been identified. As the offset is quite small, it is not of particular interest in this study and will not be considered further.

In order to better understand why the Dyer-Roeder approximation makes a much better prediction of the redshift-distance relation than the method based on spatial averages does, it is instructive to look at the different contributions to the redshift according to the general expression

$$1 + z = \exp \left(\int_t^{t_0} \Gamma dt \left(\frac{1}{3} \theta + \sigma_{\alpha\beta} e^\alpha e^\beta + \dot{u}^\alpha e_\alpha \right) \right), \quad (4.7)$$

where $e^\alpha = -\frac{k^\alpha}{k^\beta u_\beta} - u^\alpha$ is the spatial direction vector of the light ray, $\dot{u}^\alpha := u^\beta \nabla_\beta u^\alpha$ is the fluid acceleration and Γ is the lapse function which is equal to 1 in the EdS region and to A in the Schwarzschild region. These different contributions to the redshift are discussed in detail below and are shown in figure 6 along single, random light rays in model 2 and variations of model 2 with different values of r_{bie} .

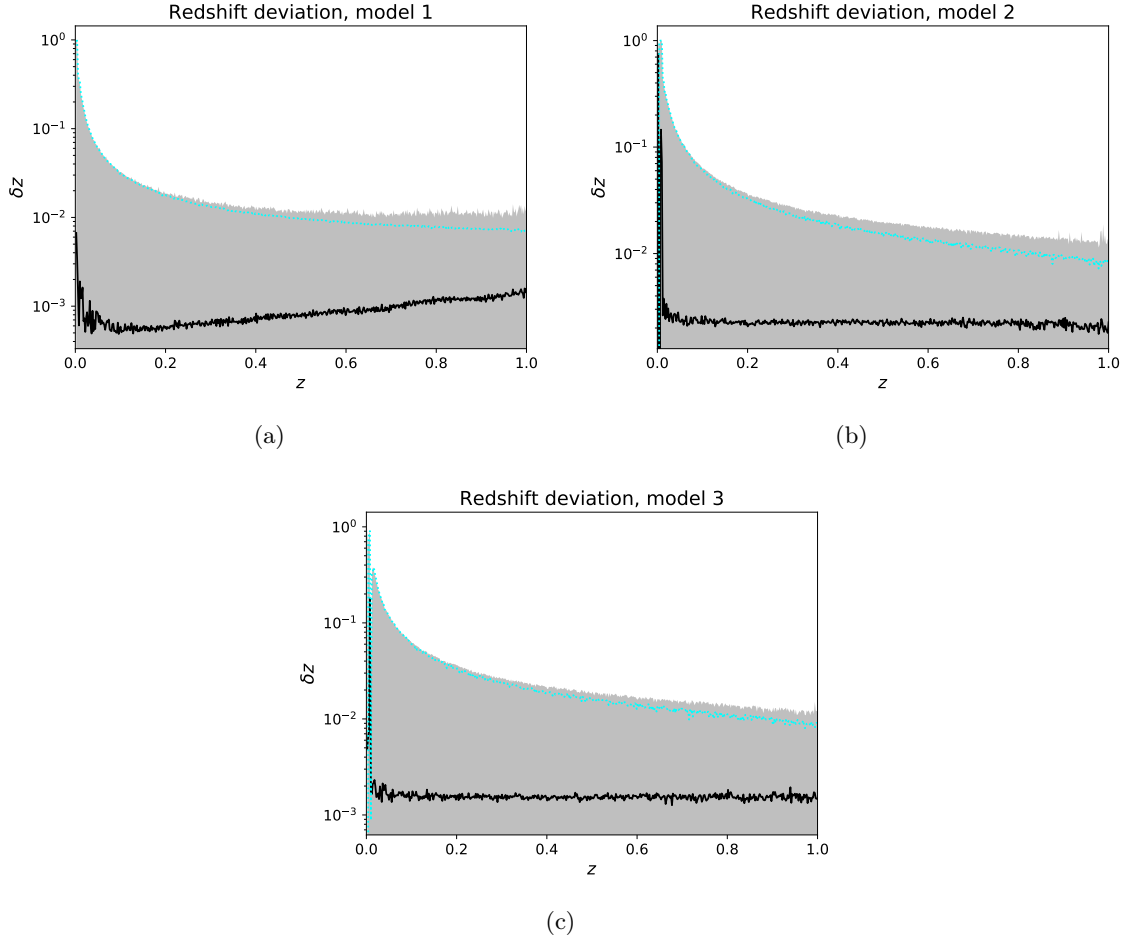


Figure 5. Fluctuations in the redshift, $\delta z := \frac{z_{\text{exact}} - z_{\text{EdS}}}{z_{\text{exact}}}$, along 1000 light rays for models 1, 2 and 3. The black line shows the mean while the shaded area shows the dispersion. The negative valued lower rim of the dispersion is indicated in cyan through absolute values.

In the Schwarzschild region, the only contribution comes from the acceleration of the source. In the exterior Schwarzschild region there is no natural velocity field to choose but in the interior region, the natural choice would be the velocity of the (comoving) fluid. This velocity field is $u_{\mu}^{\text{sch}} = (-\sqrt{A}, 0, 0, 0)$ with corresponding acceleration $\dot{u}_{\mu}^{\text{sch}} = (0, \frac{1}{2} \frac{A_{,r}}{A}, 0, 0)$. This velocity field is also chosen in the exterior Schwarzschild metric. In [32, 33], another velocity field was chosen, namely one of a free-falling observer. It does not matter much which velocity field is chosen in the Schwarzschild region; the difference between the redshift seen by different observers is a matter of a local Doppler term so the choice will not affect the redshift of light emitted by a comoving source in the EdS region and seen by the comoving observer also in the EdS region and it therefore does not affect the mean redshift significantly. One may note though that for a non-vacuum region, the velocity field of the fluid component is natural to choose not only because it is the velocity field representing the only actual source in the model, but also because this source directly affects the spacetime geometry and dynamics and therefore its velocity can be expressed through the metric functions.

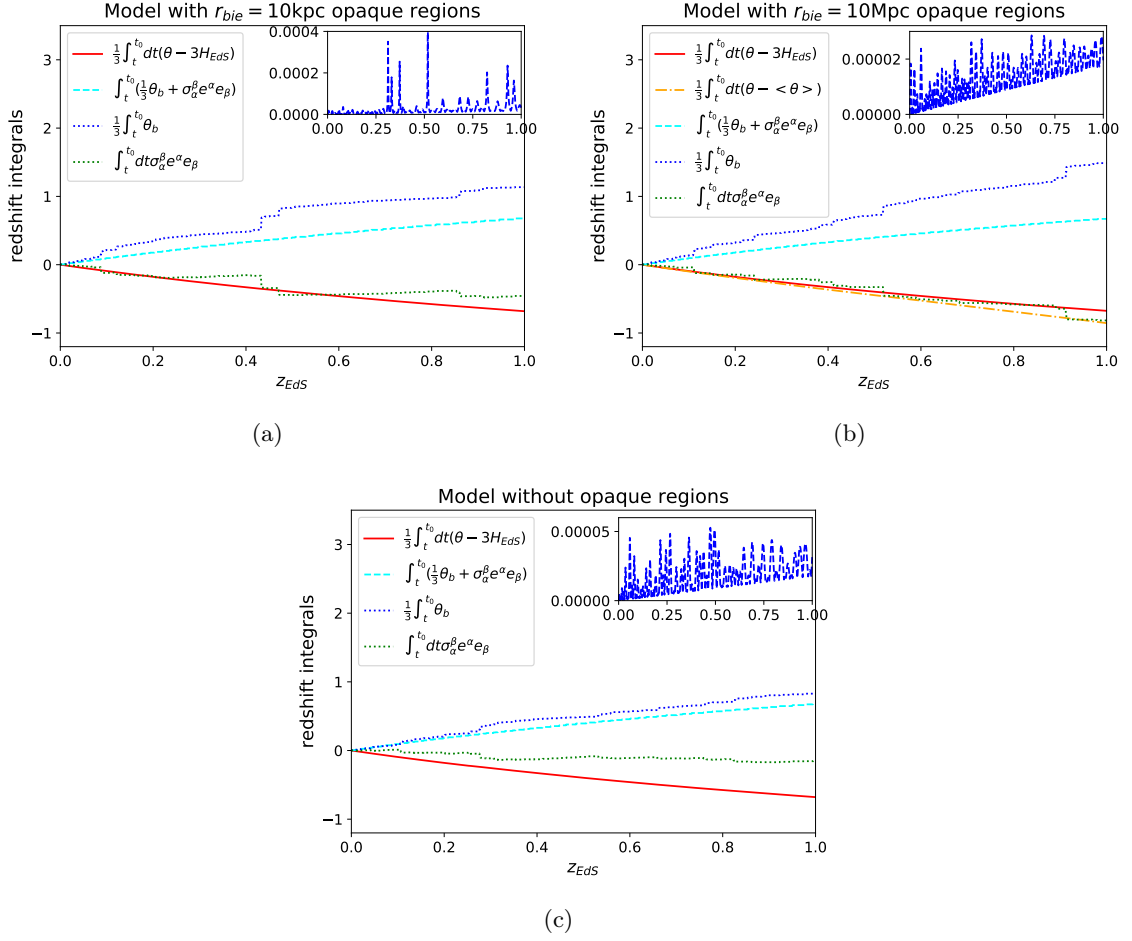


Figure 6. Redshift components along individual light rays for models with $M = 10^{16} M_{\odot}$, $\xi_0 = 26.1 \text{ Mpc}$ and different values of r_{bie} . The contribution from the acceleration, $1 + z_{\text{Sch}}$, is nearly zero so is not included in the main figures but is instead shown in separate close-ups in each subfigure. In the top right figure, the contributions from the fluctuations in the shear are shown both with respect to the background value ($3H_{\text{EdS}}$) and the spatial average with spatial averages not including opaque regions ($\langle \theta \rangle$).

The redshift contribution from a single traversal of a Schwarzschild region is given by

$$\begin{aligned}
 1 + z_{\text{sch}} &= \exp \left(\int_{t_i}^{t_o} dt \sqrt{A} \dot{u}^\alpha e_\alpha \right) = \exp \left(-\frac{1}{2} \int_{t_i}^{t_o} dt \sqrt{A} \frac{A_{,r}}{A} \frac{k^r}{u_t^{\text{Sch}} k^t} \right) \\
 &= \exp \left(\int_{r_i}^{r_o} dr \frac{1}{2} \frac{A_{,r}}{\sqrt{A}} \right) = \exp \left(\int_{r_i}^{r_o} dr \frac{d}{dr} \ln \sqrt{A} \right) = \sqrt{\frac{A(r_b(t_o))}{A(r_b(t_i))}} = \sqrt{\frac{1 - \frac{2M}{r_b(t_o)}}{1 - \frac{2M}{r_b(t_i)}}},
 \end{aligned} \tag{4.8}$$

where the subscript i indicates entry into the Schwarzschild region and o indicates exit out of it. The second equality is based on noting that the spatial part of e^μ is simply $e^i = \frac{k^i}{-k^t \sqrt{A}}$.

The expression for $1 + z_{\text{Sch}}$ found above is just the ordinary expression for the redshift in the Schwarzschild metric as seen by a comoving observer (observing a comoving source).

The overall contribution to the redshift upon traversing an entire Schwarzschild region is purely due to the expansion of the Schwarzschild region's boundary and is hence an integrated Sachs-Wolfe/Rees-Sciama effect [107–109] as was also noted in [32]. Note that the contribution fluctuates as the light ray traverses a Schwarzschild hole and that it is only upon traversal of an *entire* hole that the contribution can be considered an ISW/Reese-Sciama effect.

In the EdS region, the only contribution to the redshift is that due to the expansion. Thus, the contribution to the redshift from traversing one EdS region is

$$1 + z_{\text{EdS}} = \exp \left(\int_{T_1}^{T_2} H_{\text{EdS}} dT \right) = \frac{a_{\text{EdS}}(T_1)}{a_{\text{EdS}}(T_2)}. \quad (4.9)$$

T_1 and T_2 denote the time coordinates when the light ray enters and exits the EdS region, respectively.

The remaining contribution to the redshift comes from the boundary between the EdS and exterior Schwarzschild regions. As with the volume averages, the contribution from the boundary can be estimated by modeling the boundary as an LTB model. The details are given in appendix A where it is shown that there is a delta function contribution to the shear in addition to the delta function contribution to the expansion rate that was used earlier for computing the volume averaged expansion rate. Specifically, the shear contribution from the boundary is

$$\sigma_{\alpha}^{\beta} = \xi H_{\text{EdS}} \delta(\xi - \xi_b) \cdot \text{diag} \left(0, \frac{2}{3}, -\frac{1}{3}, -\frac{1}{3} \right). \quad (4.10)$$

The two contributions to the redshift from crossing the boundary once are thus

$$\begin{aligned} 1 + z_{\theta_b} &= \exp \left(\frac{1}{3} \int_{T_1}^{T_2} dT \xi H_{\text{EdS}} \delta(\xi - \xi_b) \right) \\ &= \exp \left(\frac{1}{3} \int_{\xi_1}^{\xi_2} d\xi \frac{k^T}{k^{\xi}} \xi H_{\text{EdS}} \delta(\xi - \xi_b) \right) \\ &= \exp \left(\frac{1}{3} \left| \frac{k^T}{k^{\xi}} \right|_{\text{b}} \xi_b H_{\text{EdS}} \right) \end{aligned} \quad (4.11)$$

and

$$\begin{aligned} 1 + z_{\sigma_b} &= \exp \left(\int_{T_1}^{T_2} dT \sigma_{\alpha}^{\beta} e^{\alpha} e_{\beta} \right) \\ &= \exp \left(\int_{T_1}^{T_2} dT \left(\frac{a^2 H_{\text{EdS}} \xi \delta(\xi - \xi_b)}{3 (k^T)^2} \left[2 (k^{\xi})^2 - \xi^2 (k^{\theta})^2 - \xi^2 \sin^2(\theta) (k^{\phi})^2 \right] \right) \right) \\ &= \exp \left(\int_{\xi_1}^{\xi_2} d\xi \left(\frac{a^2 H_{\text{EdS}} \xi \delta(\xi - \xi_b)}{3 |k^{\xi} k^T|} \left[2 (k^{\xi})^2 - \xi^2 (k^{\theta})^2 - \xi^2 \sin^2(\theta) (k^{\phi})^2 \right] \right) \right) \\ &= \exp \left(\frac{a^2 H_{\text{EdS}} \xi_b}{3 |k^T k^{\xi}|} \left[2 (k^{\xi})^2 - \xi_b^2 (k^{\theta})^2 - \xi_b^2 \sin^2(\theta) (k^{\phi})^2 \right] \Big|_{\text{b}} \right), \end{aligned} \quad (4.12)$$

where the integration limits are arbitrary, though only including the boundary once. The two contributions can be multiplied to form a simple expression by noting that the spherical symmetry of the situation implies that we can without loss of generality consider a light ray traveling in a plane with one of the angles kept constant. Keeping the polar angle constant and equal to $\pi/2$, the null condition then leads to³

$$k^\xi = \pm \frac{1}{a_{\text{EdS}}} k^T \sin(\phi_b) \quad (4.13)$$

$$k^\phi = \pm \frac{1}{a_{\text{EdS}} \xi_b} k^T \cos(\phi_b), \quad (4.14)$$

where ϕ_b is the angle of impact between the light ray and the boundary with $\phi_b = \pi/2$ corresponding to a radial light ray. We can therefore write the total boundary contribution to the redshift as

$$\begin{aligned} 1 + z_b &:= (1 + z_{\sigma_b})(1 + z_{\theta_b}) \\ &= \exp \left(\frac{1}{3} \left| \frac{k^T}{k^\xi} \right| \Big|_b \xi_b H_{\text{EdS}} + \frac{H_{\text{EdS}} \xi_b}{3 |k^T k^\xi|} \left[2 (k^T \sin(\phi_b))^2 - (k^T \cos(\phi_b))^2 \right] \Big|_b \right) \\ &= \exp(a_{\text{EdS}} H_{\text{EdS}} \xi_b \sin(\phi_b)). \end{aligned} \quad (4.15)$$

For each hole a light ray traverses, it crosses the boundary twice, so the total boundary contribution from traversing a single Schwarzschild region is

$$1 + z_{b_2} := \exp[a_{\text{EdS}}(T_{\text{in}}) H_{\text{EdS}}(T_{\text{in}}) \xi_{b_{\text{in}}} \sin(\phi_{b_{\text{in}}}) + a_{\text{EdS}}(T_{\text{out}}) H_{\text{vEdS}}(t_{\text{out}}) \xi_{b_{\text{out}}} \sin(\phi_{b_{\text{out}}})], \quad (4.16)$$

where T_{in} and T_{out} are the FLRW time coordinate values at which the light ray enters and exits the Schwarzschild region, respectively. The spherical symmetry means that $\sin(\phi_{b_{\text{in}}}) = \sin(\phi_{b_{\text{out}}})$ and since the holes are modest in size, $\xi_{b_{\text{in}}} \approx \xi_{b_{\text{out}}}$. Subscripts in(out) will therefore be omitted on these quantities in the following.

Note now that, for a light ray in EdS spacetime,

$$a_{\text{EdS}}(T_{\text{in(out)}}) \xi_b \sin(\phi_b) = a_{\text{EdS}}(T_{\text{in(out)}}) \int_{\Delta T_{\text{in(out)}}} \frac{dT}{a_{\text{EdS}}} \approx \Delta T_{\text{in(out)}}, \quad (4.17)$$

where $\Delta T_{\text{in(out)}}$ is the time it takes for the light ray to travel the comoving distance $\xi_b \sin(\phi_b)$ at $T \approx T_{\text{in(out)}}$ in the EdS spacetime. The approximation indicated by “ \approx ” in equation 4.17 corresponds to neglecting the evolution of a_{EdS} during this travel time. The EdS redshift corresponding to the time interval the light ray travels in a Schwarzschild hole can be approximated as

$$\begin{aligned} 1 + z_{\text{EdS}} &= \exp \left(\int_{T_{\text{in}}}^{T_{\text{out}}} dT H_{\text{EdS}} \right) = \exp \left(\int_{\Delta \xi} d\xi a_{\text{EdS}} H_{\text{EdS}} \right) \\ &\approx \exp(\xi_b \sin(\phi_b) [a_{\text{EdS}}(T_{\text{in}}) H_{\text{EdS}}(T_{\text{in}}) + a_{\text{EdS}}(T_{\text{out}}) H_{\text{EdS}}(T_{\text{out}})]), \end{aligned} \quad (4.18)$$

where $\Delta \xi$ represents the change in the coordinate ξ along the light ray. The approximation indicated by “ \approx ” corresponds to assuming (again) that a_{EdS} and H_{EdS} do not change during

³The possibility of writing k^α this way and using it to write the simple expression for $(1 + z_{\sigma_b})(1 + z_{\theta_b})$ given in equation 4.15 even for non-radial light rays was pointed out to the author by Pierre Fleury.

travel time into and out of the hole. In addition, the approximation requires that the travel time into and out of the Schwarzschild hole actually corresponds to $\Delta T_{\text{in(out)}}$ of equation 4.17. The latter approximation becomes better the further a light ray is from the central structure. The former approximation becomes better the less time a light ray spends in a given hole. In both cases, the approximation thus becomes better the further the light ray is from being radial. The small values of δz in figure 5 indicates that the approximation is good for all the studied models.

Figure 6 shows $1 + z_{\text{Sch}}$ for three different versions of model 2. The contribution $1 + z_{\text{Sch}}$ fluctuates noticeably with peaks where the light rays come close to the central regions where the Schwarzschild mass is concentrated. The contribution to the total redshift is negligibly small in all three models though. The fluctuations in $1 + z_{\text{Sch}}$ is an order of magnitude larger in the model with small inner region which is due to the larger deviation of A from 1 due to the higher density in the inner Schwarzschild region in this model. The accumulated $1 + z_{\text{Sch}}$ along the light rays is slightly smaller (approximately by a factor of 2.5) in the model with large opaque centers which is as expected since the light rays in this model spend less time in a given Schwarzschild region which naturally makes the contribution to $1 + z_{\text{Sch}}$ from passing through any single Schwarzschild region smaller compared to the two other models where light rays can pass closer by the centers. This highlights the most important point with the redshift analysis (also discussed in [32]): The sole contribution to the redshift from passing through a Schwarzschild region (not including the boundary), is a *small* ISW effect which is negligible compared to the boundary and background contributions. Therefore, it is largely irrelevant whether or not there are sub-regions inside the Schwarzschild region which the light rays are not permitted to traverse. Consequently, the redshift will not in general be well described through a spatial average of the expansion rate as in equation 1.3 if light rays are restricted from propagating through certain spacetime regions and spatial averages are computed by omitting these regions. It must be emphasized that the analyses in [27, 28] do not specifically address this type of situation. The results obtained here show by explicit example that the results in [27, 28] cannot in general be naively extended to this type of situation where there are opaque regions in the considered spacetime.

Another way of viewing the result from the above redshift analysis is that the main effect the Schwarzschild regions have on the redshift occur at the boundary and is thus independent of whether or not there are regions interior to the boundary that the light ray is not permitted to trace. It is then natural to consider if the result could be an artifact arising from the sharp boundary between the EdS and Schwarzschild regions. However, figure 3 in [38] indicates⁴ that the same can be expected in Szekeres [110] and LTB [104–106] Swiss-cheese models, i.e. the redshift will be well described through the expansion rate averaged over all space, regardless of whether central regions are made opaque. This is despite the Szekeres and LTB models smoothly transitioning to their FLRW backgrounds rather than having abrupt δ -function boundaries.

For completeness, the redshift-distance relation is in figure 7 shown for model 2 with the

⁴Specifically, the figure shows the contributions to the redshift along light rays in different LTB and Szekeres Swiss-cheese models. From the figure, it is seen that upon traversing an inhomogeneous region the redshift will, to a good approximation, be the same as if it had simply traveled in the background *regardless of the impact parameter*.

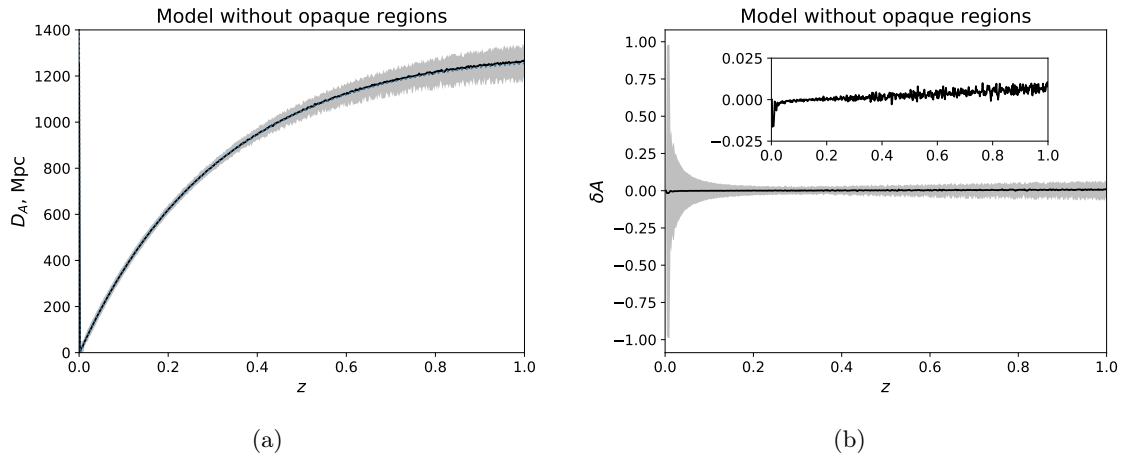


Figure 7. Mean angular diameter distance along 1000 light rays in Einstein-Straus model with transparent interior regions of $M = 10^{16} M_\odot$ and $r_{\text{bie}} = 10 \text{ Mpc}$ (i.e. model 2 with interior regions made transparent). The figure to the left shows D_A while the figure to the right shows $\delta D_A := \frac{D_A - D_{A,\text{EdS}}}{D_{A,\text{EdS}}}$. A shaded area is included to show the dispersion around the mean. A close-up is also shown in the figure to the right. The figure to the left shows D_A as a black line and $D_{A,\text{EdS}}$ as a cyan dotted line but the two lines overlap so precisely that they look like a single (black) line.

interior region made transparent. In this case, all the methods for describing the mean observations predict the same result, namely that the mean redshift-distance relation is simply that given by the EdS background and as seen in the figure, this prediction is correct. Note though, that the dispersion around the mean is much larger here than in the corresponding model with opaque interiors. This is because the light rays are much more affected by shear in the case of transparent interiors.

4.2 Redshift drift

It was above found that the mean redshift is described well by the background EdS model and not the spatial average of the regions that the light rays were permitted to traverse. This could be interpreted as indicating that the redshift depends mostly on local quantities at the spacetime points of emission and observation. However, the relation between k_0^μ and k_e^μ depends on the light path and therefore the redshift must also to some extent depend on the particular light ray's path between the source and observer and not solely on the local qualities of spacetime at the points of emission and observation. This claim is in fact in agreement with the results found above, namely that the redshift in the Schwarzschild region is very different from the redshift in a pure Schwarzschild model while the redshift in the EdS region is only modified slightly compared to in a pure EdS spacetime - in accordance with the Schwarzschild region affecting k^μ very modestly compared to the EdS region.

The redshift drift is more a local quantity than the redshift because the redshift drift depends on the derivatives $\frac{dk^T}{d\lambda}$ and not only fractions of k^T . Since $\frac{dk^T}{d\lambda} \neq k^T k_{;T}^T$ in general and because k^α depends on an integral along the light ray, the redshift drift also depends to some extent on the spacetime along the individual light rays and not only on local quantities. It is therefore interesting to look at the mean redshift drift in exact, inhomogeneous solutions to the Einstein equations, in order to learn about the behavior of redshift drift.

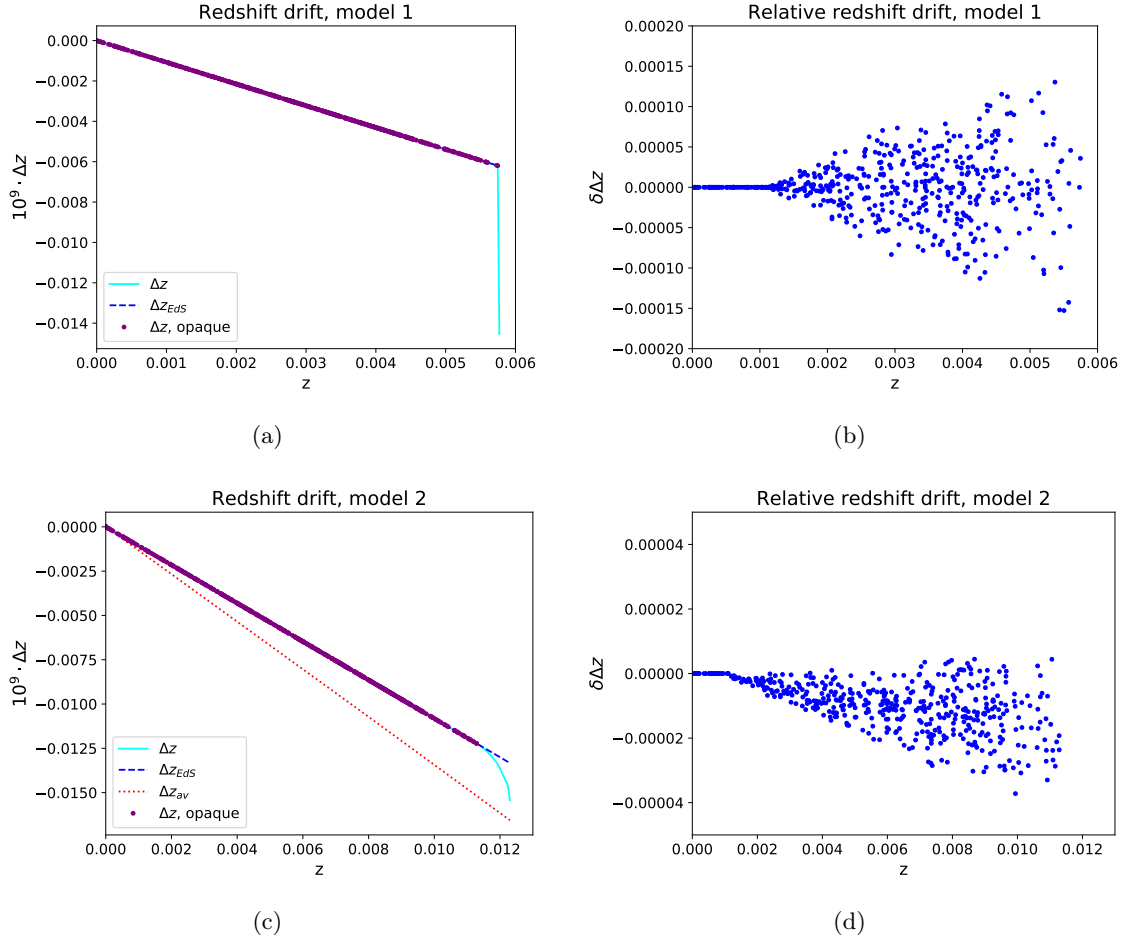


Figure 8. Redshift drift along light rays after traversing a single Schwarzschild region at different angles, with more radial impact parameters indicated by larger redshift. The top figures are for model 1 while the bottom figures are for the model 2. The figures to the left show the redshift drift for $\delta T_0 = 30$ years, scaled by a factor of 10^9 . The thick solid lines (overlapping dots, really) represent light rays that have not entered the interior Schwarzschild region and are thus labeled as “opaque”. The figures to the right show $\delta \Delta z := \frac{\delta z - \delta z_{\text{EdS}}}{\delta z_{\text{EdS}}}$ and only depicts results for light rays that have not traveled through an interior Schwarzschild region.

Figure 8 shows the redshift drift of 500 light rays after traversing a single Schwarzschild structure once with different impact parameters. The results are shown for models 1 and 2. The redshift drift is shown as a function of the value of the redshift after traversing the structure, where a larger redshift indicates a longer travel time and hence that the impact with the Schwarzschild metric has been with a more direct (radial) angle. The thick lines show the redshift drift for light rays that have not traveled through the interior regions and thus indicate the results for the opaque models. The thin cyan lines represent the models with transparent interiors and hence include light rays that have traveled through the interior regions. Clearly, the redshift drift is significantly altered along light rays that travel through the structures, but for the models with opaque regions, the redshift drift is modified very little compared to the EdS prediction. In fact, the dispersion seen in the subfigures to the right in figure 8 is a manifestation of the precision (10^{-16}) of the computations being reached.

Note that for model 1, Δz_{EdS} and Δz_{av} are identical and hence only Δz_{EdS} is shown. For model 2, the difference between the two is clear and Δz_{av} gives a poor description of Δz (as expected considering the results found earlier regarding the mean redshift). For this reason, the quantity $\frac{\Delta z - \Delta z_{\text{av}}}{\Delta z_{\text{av}}}$ is not computed.

The results presented in figure 8 imply that the redshift drift will be well approximated by Δz_{EdS} in Einstein-Straus models if the interior regions are opaque. If on the other hand the interior regions are not opaque the mean will deviate from Δz_{EdS} . However, the fraction of light rays that will traverse significantly into the interior Schwarzschild region will be modest so the bias will presumably not be very big. Indeed, the mean of the $\delta\Delta z$ for the results shown in figure 8 for the two models with transparent interiors are approximately 0.0026 ($= 10^{15} M_{\odot}$) and 0.0011 ($= 10^{16} M_{\odot}$). For the opaque versions, the means are $5.5 \cdot 10^{-7}$ and $9.5 \cdot 10^{-6}$. The means of the opaque models are several orders of magnitudes smaller than for the transparent models but even for the transparent models, the means are quite modest (sub-percent). The accumulated effect of the structures on the redshift drift after traversing many structures will therefore presumably be modest despite the striking behavior for light rays traversing through the interiors.

The prominent deviation between Δz_{EdS} and Δz for light rays traversing the interior Schwarzschild regions is striking and merits further consideration. However, to meaningfully consider it further requires using model setups reminiscent of the relevant real scenario, i.e. light rays traversing through realistic regions with sources and observer position realistic compared to the sources expected to be used for redshift drift measurements in the future. This is beyond the scope of the work presented here. Note especially that the large deviation from Δz_{EdS} is due to $k_{;T}^T k^T$ beginning to deviate from $\frac{dK^T}{d\lambda}$. Since this apparently happens (significantly) only from propagating in the interior Schwarzschild region and not already when propagating through the exterior Schwarzschild region, the effect must depend crucially on the exact form of the metric functions. A meaningful quantification of the effect therefore requires using a realistic interior region (if it can be justified physically to let light rays travel through the interior regions at all).

4.3 Note on interior FLRW regions

As mentioned in section 2, an FLRW metric can be joined with the Schwarzschild metric in such a way that the FLRW metric is interior to the vacuum Schwarzschild region. The boundary between the interior FLRW metric and the exterior Schwarzschild metric is analogous to the boundary between the exterior FLRW region and the exterior Schwarzschild region. Therefore, the redshift-distance results obtained above do not change much if an interior FLRW region is included. Specifically, the average expansion rate will still be that of the exterior FLRW region: Denoting the radial coordinate of the inner FLRW region by $\bar{\xi}$, the average expansion rate is

$$\begin{aligned} \langle \theta \rangle &= \frac{(\xi_0^3 - \xi_b^3) H_b + \int_b d\xi H_b \delta(\xi - \xi_b) \xi^3 + \bar{\xi}_{\text{bie}}^3 H_{\text{bie}} - \int_{\text{bie}} d\bar{\xi} H_{\text{bie}} \delta(\bar{\xi} - \bar{\xi}_{\text{bie}}) \bar{\xi}^3}{\frac{1}{3} \xi_0^3} \\ &= \frac{\xi_0^3 H_b + \bar{\xi}_{\text{bie}}^3 H_{\text{bie}} - \bar{\xi}_{\text{bie}}^3 H_{\text{bie}}}{\frac{1}{3} \xi_0^3} = 3H_b, \end{aligned} \quad (4.19)$$

where subscripts b indicate FLRW values on the outer boundary, and bie on the inner boundary. Integrals \int_{ξ_b} are integrals over an interval that contains $\xi = \xi_b$ and similarly for $\int_{\bar{\xi}_{\text{bie}}}$.

The reason that the average expansion rate is still that of the outer FLRW region is that the expansion rate contribution from the inner FLRW region cancels with the contribution from the inner boundary. The same thing happens when computing the redshift: There is a non-negligible redshifting of light as it propagates through the inner FLRW region, but this is largely canceled by the effects from the inner boundary (see the discussion around equations 4.11-4.18).

See e.g. [111–113] for early studies on light propagation in models with both inner and outer FLRW regions joined through a Schwarzschild vacuum.

5 Summary

Several particular Einstein-Straus models were studied in terms of their light propagation qualities in order to compare mean observations with predictions based on spatial averaging and the Dyer-Roeder approximation. In agreement with earlier studies, it was shown with explicit examples that the Dyer-Roeder approximation gives a good description of the mean redshift-distance relation when contributions from shear is small. It was also shown that the relation based on spatial averages gives the same prediction as the Dyer-Roeder approximation in models with parameter values similar to those of earlier studies. When choosing a setup where the two approximations differ significantly, it was found that the Dyer-Roeder approximation gives the correct result while the method based on spatial averages underestimates the angular diameter distance significantly at high redshift. This shows that the relations obtained in [27, 28], where the redshift-distance relation is based on spatially averaged quantities, cannot be naively generalized to spacetimes with opaque regions. While the results shown here are specifically based on Einstein-Straus models, results presented earlier (figure 3 in [38]) indicate that this is the case for any Swiss-cheese model. It is important to learn how relevant these results are for real observations, i.e. which observables should be considered based on light rays propagating through a universe with opaque regions, what is the size and mass of these regions, and do the results presented here describe such opaque regions in terms of their effects on mean observations in general or are the results found here a specific feature of the Swiss-cheese models.

6 Acknowledgments

The author thanks Pierre Fleury for comments on the manuscript and explanations regarding results presented in [33]. The work was completed using computer resources from the Finnish Grid and Cloud Infrastructure urn:nbn:fi:research-infras-2016072533.

During the preparation of the original manuscript, the author was supported by the Independent Research Fund Denmark under grant number 7027-00019B.

During the final stages of review, the author transitioned to being supported by the Carlsberg foundation. Final numerical checks made during this stage utilized UCloud services provided by SDU eScience Center.

A Boundary contributions to expansion rate and shear

This appendix serves to compute the contributions to the shear and expansion rate on the boundary between EdS and Schwarzschild regions by describing the region through a Lemaitre-Tolman-Bondi (LTB) model [104–106].

The LTB model is a spherically symmetric dust solution to the Einstein equations. Its line element can be written as

$$ds^2 = -dt^2 + \frac{R_{,\xi}^2(t, \xi)}{1 - k(\xi)} d\xi^2 + R^2(t, \xi) d\Omega^2. \quad (\text{A.1})$$

The metric function R can be considered an FLRW scale factor generalized to include radial dependence. This is seen through the dynamical equation $R_{,t}^2 = \frac{2M}{R} - k$.

A straightforward computation shows that the local expansion rate and shear tensor components are given by

$$\theta = 2 \frac{R_{,t}}{R} + \frac{R_{,t\xi}}{R_{,\xi}} \quad (\text{A.2})$$

$$\sigma_\alpha^\beta = \text{diag} \left(0, \frac{2}{3}, -\frac{1}{3}, -\frac{1}{3} \right) \left(\frac{R_{,t\xi}}{R_{,\xi}} - \frac{R_{,t}}{R} \right) \quad (\text{A.3})$$

One may construct an LTB model consisting of a central static region surrounded by an EdS spacetime. The transition between the two regions can be constructed e.g. using a function that transitions smoothly between the two spacetimes. The transition between the two regions can be made as fast (in the radial direction) as one wishes, with the limit being a Heaviside function-like transition. This is the case that best corresponds to the situation in the Swiss cheese models studied in the main text, where the transition between EdS and Schwarzschild spacetimes occurs at a specific ξ -value rather than smoothly over an extended ξ -interval. In this case, $R_{,t}$ can be approximated as $\Theta(\xi_b) a_{,t}^{EdS} \xi$, where $\Theta(\xi_b)$ is the Heaviside function. The non-vanishing expansion rate of this model is

$$\begin{aligned} \theta(\xi \geq \xi_b) &= 2 \frac{a_{,t}^{EdS}}{a^{EdS}} + \frac{a_{,t}^{EdS} + \xi \delta(\xi - \xi_b) a_{,t}^{EdS}}{a^{EdS}} \\ &= 3H_{\text{EdS}} + \xi \delta(\xi - \xi_b) H_{\text{EdS}}, \end{aligned} \quad (\text{A.4})$$

where $\delta(\xi - \xi_b)$ is the delta function, entering into the expression as the derivative of the Heaviside function. Similarly, the shear is

$$\sigma_\alpha^\beta = \text{diag} \left(0, \frac{2}{3}, -\frac{1}{3}, -\frac{1}{3} \right) \xi H_{\text{EdS}} \delta(\xi - \xi_b). \quad (\text{A.5})$$

The boundary contributions (proportional to $\delta(\xi - \xi_b)$) can be used to estimate the boundary contributions of shear and expansion rate in the Swiss-cheese models studied in the main text.

References

- [1] Planck Collaboration, Planck 2018 results. I. Overview and the cosmological legacy of Planck, arXiv:1807.06205v2 [astro-ph.CO]

- [2] Adam G. Riess, The Expansion of the Universe is Faster than Expected, *Nat Rev Phys* 2, 10-12, 2020, arXiv:2001.03624v1 [astro-ph.CO]
- [3] Thomas Buchert, Alan A. Coley, Hagen Kleinert, Boudewijn F. Roukema, David L. Wiltshire, Observational Challenges for the Standard FLRW Model, *Int. J. Mod. Phys. D* 25, 1630007 (2016), arXiv:1512.03313v2 [astro-ph.CO]
- [4] Eleonora Di Valentino, Alessandro Melchiorri, Joseph Silk, Cosmic Discordance: Planck and luminosity distance data exclude LCDM, arXiv:2003.04935v1 [astro-ph.CO]
- [5] Eleonora Di Valentino, Alessandro Melchiorri, Joseph Silk, Planck evidence for a closed Universe and a possible crisis for cosmology, *Nature Astronomy* volume 4, pages 196–203 (2020), arXiv:1911.02087v1 [astro-ph.CO]
- [6] W. Handley, Curvature tension: evidence for a closed universe, arXiv:1908.09139
- [7] G. F. R. Ellis and W. Stoeger, the 'fitting problem' in cosmology, *Class. Quantum Grav.* 4 1697-1729 (1987)
- [8] G. F. R. Ellis. Relativistic cosmology - Its nature, aims and problems. In B. Bertotti, F. de Felice and A. Pascolini, editor, *General Relativity and Gravitation Conference*, pages 215–288, Dordrecht (1984)
- [9] Nick Kaiser, John A. Peacock, On the Bias of the Distance-Redshift Relation from Gravitational Lensing, *MNRAS* 455, 4518–4547 (2016), arXiv:1503.08506v1 [astro-ph.CO]
- [10] I. Ben-Dayan, G. Marozzi, F. Nugier, and G. Veneziano, The second-order luminosity-redshift relation in a generic inhomogeneous cosmology, *JCAP* 11 (Nov., 2012) 45, arXiv:1209.4326
- [11] G. Fanizza, M. Gasperini, G. Marozzi, and G. Veneziano, An exact Jacobi map in the geodesic light-cone gauge, *JCAP* 11 (Nov., 2013) 019, arXiv:1308.4935
- [12] G. Fanizza, M. Gasperini, G. Marozzi, and G. Veneziano, A new approach to the propagation of light-like signals in perturbed cosmological backgrounds, *JCAP* 8 (Aug., 2015) 20, arXiv:1506.02003
- [13] O. Umeh, C. Clarkson, and R. Maartens, Nonlinear relativistic corrections to cosmological distances, redshift and gravitational lensing magnification: I. Key results, *Classical and Quantum Gravity* 31 (Oct., 2014) 202001, arXiv:1207.2109
- [14] O. Umeh, C. Clarkson, and R. Maartens, Nonlinear relativistic corrections to cosmological distances, redshift and gravitational lensing magnification: II. Derivation, *Classical and Quantum Gravity* 31 (Oct., 2014) 205001, arXiv:1402.1933
- [15] Hamish G. Rose, Apparent magnitudes in an inhomogeneous universe: the global viewpoint, *Astrophys.J.* 560 (2001) L15-L18, arXiv:astro-ph/0106489v2
- [16] T.W.B. Kibble, Richard Lieu, Average magnification effect of clumping of matter, *Astrophys.J.* 632 (2005) 718-726, arXiv:astro-ph/0412275v2
- [17] Krzysztof Bolejko, Weak lensing and the Dyer-Roeder approximation, *MNRAS* 412, 1937 (2011), arXiv:1011.3876v1 [astro-ph.CO]
- [18] Syksy Rasanen, Light propagation and the average expansion rate in near-FRW universes, *Phys. Rev. D* 85, 083528 (2012), arXiv:1107.1176v2 [astro-ph.CO]
- [19] T. Futamase and M. Sasaki, Light propagation and the distance-redshift relation in a realistic inhomogeneous universe, *Phys. Rev. D* 40, 2502 (1989)
- [20] Misao Sasaki, Cosmological gravitational lens equation - Its validity and limitation, *Progr. Theor. phys.*, Vol 90, No.4, 753-781 (1993)
- [21] A. A. Coley, Null geodesics and observational cosmology, arXiv:0812.4565v1 [astro-ph]
- [22] A. A. Coley, Cosmological Observations: Averaging on the Null Cone, arXiv:0905.2442v1 [gr-qc]

- [23] Eric V. Linder, Transition from Clumpy to Smooth Angular Diameter Distances, THE ASTROPHYSICAL JOURNAL, 497:28-31, 1998, arXiv:astro-ph/9707349v2
- [24] C. C. Dyer and R. C. Roeder, The Distance-Redshift Relation for Universes with no Intergalactic Medium, Astrophys. J. 174, L115 (1972)
- [25] C. C. Dyer and R. C. Roeder, Distance-redshift relations for universes with some intergalactic medium, Astrophys. J. 180, L31 (1973)
- [26] Y. B. Zeldovich, Observations in a Universe Homogeneous in the Mean, Soviet Astronomy 8 (1964) 13
- [27] Syksy Rasanen, Light propagation in statistically homogeneous and isotropic dust universes, JCAP 0902:011,2009, arXiv:0812.2872v2 [astro-ph]
- [28] Syksy Rasanen, Light propagation in statistically homogeneous and isotropic universes with general matter content, JCAP 1003:018,2010, arXiv:0912.3370v2 [astro-ph.CO]
- [29] Chris Clarkson et al., (Mis-)Interpreting supernovae observations in a lumpy universe, Monthly Notices of the Royal Astronomical Society, Volume 426, Issue 2, pp. 1121-1136 (2012), arXiv:1109.2484v3 [astro-ph.CO]
- [30] E. V. Linder, Light propagation in generalized Friedmann universes, Astron. Astrophys. 206, 190-198 (1988)
- [31] Eric V. Linder, Averaging Inhomogeneous Universes: Volume, Angle, Line of Sight, arXiv:astro-ph/9801122v2
- [32] Pierre Fleury, Swiss-cheese models and the Dyer-Roeder approximation, JCAP 06 (2014) 054, arXiv:1402.3123v3 [astro-ph.CO]
- [33] Pierre Fleury, Helene Dupuy, Jean-Philippe Uzan: Interpretation of the Hubble diagram in a nonhomogeneous universe, Physical Review D 87, 123526 (2013), arXiv:1302.5308v2 [astro-ph.CO]
- [34] Kantowski R, Corrections in the Luminosity-Redshift Relations of the Homogeneous Friedmann Models, 1969 Astrophys. J. 155 89
- [35] Krzysztof Bolejko: The Szekeres Swiss Cheese model and the CMB observations, Gen.Rel.Grav.41:1737-1755,2009, arXiv:0804.1846v2 [astro-ph]
- [36] Krzysztof Bolejko, Marie-Noelle Celerier: Szekeres Swiss-Cheese model and supernova observations, Phys.Rev.D82:103510,2010,
- [37] Austin Peel, M. A. Troxel, Mustapha Ishak: Effect of inhomogeneities on high precision measurements of cosmological distances, Phys. Rev. D 90, 123536 (2014), arXiv:1408.4390v2 [astro-ph.CO]
- [38] S. M. Koksang, Light propagation in Swiss cheese models of random close-packed Szekeres structures: Effects of anisotropy and comparisons with perturbative results, Phys. Rev. D 95, 063532 (2017), arXiv:1703.03572
- [39] S. M. Koksang, Towards statistically homogeneous and isotropic perfect fluid universes with cosmic backreaction, Class. Quantum Grav. 36 185004, 2019, arXiv:1907.08681
- [40] Anthony Nwankwo, Mustapha Ishak, John Thompson, Luminosity distance and redshift in the Szekeres inhomogeneous cosmological models, JCAP 1105:028, 2011, arXiv:1005.2989v3 [astro-ph.CO]
- [41] Norimasa Sugiura, Ken-ichi Nakao, Daisuke Ida, Nobuyuki Sakai, Hideki Ishihara: How Do Nonlinear Voids Affect Light Propagation?, Prog.Theor.Phys. 103 (2000) 73-89, arXiv:astro-ph/9912414v1
- [42] N. Brouzakis, N. Tetradis, E. Tzavara: The Effect of Large-Scale Inhomogeneities on the Luminosity Distance, JCAP 0702:013,2007, arXiv:astro-ph/0612179v2

- [43] Nikolaos Brouzakis, Nikolaos Tetradis, Eleftheria Tzavara: Light Propagation and Large-Scale Inhomogeneities, JCAP0804:008,2008, arXiv:astro-ph/0703586v4
- [44] Tomohiro Kai, Hiroshi Kozaki, Ken-ichi nakao, Yasusada Nambu, Chul-Moon Yoo: Can inhomogeneities accelerate the cosmic volume expansion?, Prog.Theor.Phys.117:229-240,2007, arXiv:gr-qc/0605120v2
- [45] Valerio Marra, Edward W. Kolb, Sabino Matarrese, Antonio Riotto: On cosmological observables in a swiss-cheese universe, Phys.Rev.D76:123004,2007, arXiv:0708.3622v3 [astro-ph]
- [46] Valerio Marra, Edward W. Kolb, Sabino Matarrese: Light-cone averages in a swiss-cheese universe, Phys.Rev.D77:023003,2008, arXiv:0710.5505v2 [astro-ph]
- [47] Valerio Marra, Alessio Notari: Observational constraints on inhomogeneous cosmological models without dark energy, Class. Quantum Grav. 28 (2011) 164004, arXiv:1102.1015v2 [astro-ph.CO]
- [48] Tirthabir Biswas, Alessio Notari: "Swiss-Cheese" Inhomogeneous Cosmology & the Dark Energy Problem, JCAP 0806:021,2008, arXiv:astro-ph/0702555v1
- [49] Timothy Clifton, Joe Zuntz: Hubble Diagram Dispersion From Large-Scale Structure, Mon. Not. R. Astron. Soc. 400 (2009) 2185, arXiv:0902.0726v2 [astro-ph.CO]
- [50] Wessel Valkenburg: Swiss Cheese and a Cheesy CMB, JCAP06(2009)010, arXiv:0902.4698v3 [astro-ph.CO]
- [51] Valentin Kostov: Average luminosity distance in inhomogeneous universes, JCAP 1004:001,2010, arXiv:0910.2611v3 [astro-ph.CO]
- [52] Sebastian J. Szybka: On light propagation in Swiss-Cheese cosmologies, Phys.Rev.D84:044011,2011, arXiv:1012.5239v2 [astro-ph.CO]
- [53] Krzysztof Bolejko: The effect of inhomogeneities on the distance to the last scattering surface and the accuracy of the CMB analysis, JCAP 02(2011)025, arXiv:1101.3338v1 [astro-ph.CO]
- [54] R. Ali Vanderveld, Eanna E. Flanagan, Ira Wasserman: Luminosity distance in "Swiss cheese" cosmology with randomized voids: I. Single void size, Phys.Rev.D78:083511,2008, arXiv:0808.1080v2 [astro-ph]
- [55] Eanna E. Flanagan, Naresh Kumar, Ira Wasserman, R. Ali Vanderveld: Luminosity distance in Swiss cheese cosmology with randomized voids. II. Magnification probability distributions, Phys.Rev.D85:023510,2012, arXiv:1109.1873v2 [gr-qc]
- [56] Sofie Marie Kocsbang, Chris Clarkson, Accurately computing weak lensing convergence, MNRAS 486 L41-L45 (2019), arXiv:1812.00861
- [57] S. M. Kocsbang, Light path averages in spacetimes with non-vanishing average spatial curvature, Phys. Rev. D 100, 063533 (2019), arXiv:1909.00610
- [58] Daniele Gregoris, Kjell Rosquist, Observational backreaction in discrete black holes lattice cosmological models, arXiv:2006.00855 [gr-qc]
- [59] Timothy Clifton, Pedro G. Ferreira, Archipelagian Cosmology: Dynamics and Observables in a Universe with Discretized Matter Content, Phys.Rev.D80:103503,2009; Phys.Rev.D84:109902,2011, arXiv:0907.4109v3 [astro-ph.CO]
- [60] Timothy Clifton, Pedro G. Ferreira, Errors in Estimating Ω_Λ due to the Fluid Approximation, JCAP 0910:26,2009, arXiv:0908.4488v2 [astro-ph.CO]
- [61] Timothy Clifton, Pedro G. Ferreira, Kane O'Donnell, An Improved Treatment of Optics in the Lindquist-Wheeler Models, Phys. Rev. D 85, 023502 (2012), arXiv:1110.3191v2 [astro-ph.CO]
- [62] Jean-Philippe Bruneton, Julien Larena, Observables in a lattice Universe, Class. Quantum Grav. 30 (2013) 025002, arXiv:1208.1411v2 [gr-qc]

- [63] J. Larena, The fitting problem in a lattice Universe, arXiv:1210.2161v1 [astro-ph.CO]
- [64] E. Mortsell, The Dyer-Roeder distance-redshift relation in inhomogeneous universes, *A&A* 382, 787-791 (2002), arXiv:astro-ph/0109197v1
- [65] Pierre Fleury, Julien Larena, Jean-Philippe Uzan, The theory of stochastic cosmological lensing, *JCAP* 11 (2015) 022, arXiv:1508.07903v2 [gr-qc]
- [66] John T. Giblin Jr, James B. Mertens, Glenn D. Starkman, Observable Deviations from Homogeneity in an Inhomogeneous Universe, *The Astrophysical Journal*, 833:247 (8pp), 2016, arXiv:1608.04403v2 [astro-ph.CO]
- [67] Eloisa Bentivegna, Mikolaj Korzynski, Ian Hinder, Daniel Gerlicher, Light propagation through black-hole lattices, *Journal of Cosmology and Astroparticle Physics*, 1703, 014 (2017), arXiv:1611.09275v2 [gr-qc]
- [68] Kenji Tomita, Angular Diameter Distances in Clumpy Friedmann Universes, *Prog.Theor.Phys.* 100 (1998) 79-90, arXiv:astro-ph/9806047v1
- [69] Ryuichi Takahashi, Masamune Oguri, Masanori Sato, Takashi Hamana, Probability Distribution Functions of Cosmological Lensing: Convergence, Shear, and Magnification, *The Astrophysical Journal*, 742:15 (15pp), (2011), arXiv:1106.3823v2 [astro-ph.CO]
- [70] Krzysztof Bolejko, Pedro G. Ferreira, Ricci focusing, shearing, and the expansion rate in an almost homogeneous Universe, *JCAP*05(2012)003, arXiv:1204.0909v2 [astro-ph.CO]
- [71] Francesca Lepori, Julian Adamek, Ruth Durrer, Chris Clarkson, Louis Coates, Weak-lensing observables in relativistic N-body simulations, arXiv:2002.04024v1 [astro-ph.CO]
- [72] Thomas Buchert: On average properties of inhomogeneous fluids in general relativity I: dust cosmologies, *Gen.Rel.Grav.* 32 (2000) 105-125, arXiv:gr-qc/9906015v2
- [73] Thomas Buchert: On average properties of inhomogeneous fluids in general relativity II: perfect fluid cosmologies, *Gen.Rel.Grav.*33:1381-1405,2001 , arXiv:gr-qc/0102049v2
- [74] Julien Larena et al.: Testing backreaction effects with observations, *Phys.Rev.D*79:083011,2009, arXiv:0808.1161v2 [astro-ph]
- [75] Eran Rosenthal, Eanna E. Flanagan: Cosmological backreaction and spatially averaged spatial curvature, arXiv:0809.2107v1 [gr-qc]
- [76] Aseem Paranjape, T. P. Singh: Explicit Cosmological Coarse Graining via Spatial Averaging, *Gen.Rel.Grav.*40:139-157,2008, arXiv:astro-ph/0609481v4
- [77] David L. Wiltshire, Cosmic clocks, cosmic variance and cosmic averages, *NewJ.Phys.*9:377,2007, arXiv:gr-qc/0702082v4
- [78] David L. Wiltshire, Exact solution to the averaging problem in cosmology, *Phys.Rev.Lett.*99:251101,2007, arXiv:0709.0732v2 [gr-qc]
- [79] David L. Wiltshire, Cosmological equivalence principle and the weak-field limit, *Phys.Rev.D*78:084032,2008, arXiv:0809.1183v3 [gr-qc]
- [80] David L. Wiltshire, Average observational quantities in the timescape cosmology, *Phys.Rev.D*80:123512,2009, arXiv:0909.0749v2 [astro-ph.CO]
- [81] Peter R. Smale, David L. Wiltshire, Supernova tests of the timescape cosmology, *Mon. Not. R. Astron. Soc.* 413 (2011) 367-385, arXiv:1009.5855v2 [astro-ph.CO]
- [82] David L. Wiltshire, What is dust? - Physical foundations of the averaging problem in cosmology, *Class.Quant.Grav.*28:164006, 2011, arXiv:1106.1693v1 [gr-qc]
- [83] Phillip Helbig, Calculation of distances in cosmological models with small-scale inhomogeneities and their use in observational cosmology: a review, *The Open Journal of Astrophysics*, 2020, volume 3, issue 1, id 1, arXiv:1912.12269v1 [astro-ph.CO]

- [84] Teppo Mattsson, Dark energy as a mirage, *Gen.Rel.Grav.*42:567-599,2010, arXiv:0711.4264v3 [astro-ph]
- [85] J. Ehlers, P. Schneider, Self-consistent probabilities for gravitational lensing in inhomogeneous universes, *Astron. astrophys.* 168, 57-61 (1986)
- [86] V. C. Busti, R. F. L. Holanda, C. Clarkson, Supernovae as probes of cosmic parameters: estimating the bias from under-dense lines of sight, *JCAP*11(2013)020, arXiv:1309.6540v2 [astro-ph.CO]
- [87] P. Schneider, J. Ehlers, E. E. Falco, *Gravitational Lenses* (study edition), Springer-Verlag Berlin heidelberg New York, 2nd printing, 1999
- [88] A. Einstein and E. G. Straus, *Reviews of Modern Physics* 17, 120 (1945)
- [89] Jean-Philippe Uzan, Chris Clarkson, George F.R. Ellis, Time drift of cosmological redshifts as a test of the Copernican principle, *Phys.Rev.Lett.*100:191303,2008, arXiv:0801.0068v2 [astro-ph]
- [90] Chul-Moon Yoo, Tomohiro Kai, Ken-ichi Nakao, Redshift Drift in LTB Void Universes, *Phys.Rev.D*83:043527,2011, arXiv:1010.0091v1 [astro-ph.CO]
- [91] Priti Mishra, Marie-Noelle Celerier, Redshift and redshift-drift in $\Omega=0$ quasi-spherical Szekeres cosmological models and the effect of averaging, arXiv:1403.5229v1 [astro-ph.CO]
- [92] Priti Mishra, Marie-Noelle Celerier, Tejinder P. Singh, Redshift drift in axially symmetric quasi-spherical Szekeres models, *Phys. Rev. D* 86, 083520 (2012), arXiv:1206.6026v2 [astro-ph.CO]
- [93] Priti Mishra, Marie-Noelle Celerier, Tejinder P. Singh, Redshift-drift as a test for discriminating between decelerating inhomogeneous and accelerating universe models, arXiv:1301.4358v2 [astro-ph.CO]
- [94] Adam Balcerzak, Mariusz P. Dabrowski, Redshift drift in a pressure-gradient cosmology, *Phys. Rev. D* 87, 063506 (2013), arXiv:1210.6331v4 [astro-ph.CO]
- [95] Pierre Fleury, Cyril Pitrou, Jean-Philippe Uzan, Light propagation in a homogeneous and anisotropic universe, *Phys. Rev. D* 91, 043511 (2015), arXiv:1410.8473v3 [gr-qc]
- [96] S. M. Koksang, Observations in statistically homogeneous, locally inhomogeneous cosmological toy-models without FLRW backgrounds, *MNRAS* 498, L135-L139 (2020), arXiv:2008.07108 [astro-ph.CO]
- [97] S. M. Koksang, Another look at redshift drift and the backreaction conjecture, *JCAP*10(2019)036, arXiv:1909.13489v1 [astro-ph.CO]
- [98] Andrzej Krasinski, *Inhomogeneous cosmological models*, Cambridge university press, 1997
- [99] M. P. Hobson, G. Efstathiou, A. N. Lasenby, *General relativity An introduction for physicists*, Cambridge University Press, 7th printing, 2014
- [100] G. Darrois, *Memorial des sciences mathematiques*, fascicule 25 (1927) 1, p. 28
For a source in English, see e.g. W. B. Bonnor and P. A. Vickers, *Junction Conditions in General Relativity*, *General Relativity and Gravitation*, Vol. 13, No. 1, 1981
- [101] Mustapha Ishak, Wolfgang Rindler, The Relevance of the Cosmological Constant for Lensing, *Gen. Rel. Grav.* 42: 2247-2268, 2010, arXiv:1006.0014v1 [astro-ph.CO]
- [102] Stella Seitz, Peter Schneider, Juergen Ehlers, Light Propagation in Arbitrary Spacetimes and the Gravitational Lens Approximation, *Class.Quant.Grav.*11:2345-2374,1994, arXiv:astro-ph/9403056v1
- [103] S. M. Koksang, S. Hannestad, Redshift drift in an inhomogeneous universe: averaging and the backreaction conjecture, *JCAP*01(2016)009, arXiv:1512.05624v2 [astro-ph.CO]
- [104] G. Lemaitre, *L'Univers en expansion*, *Annales de la Societe Scienti*

- que de Bruxelles A 53, 51 (1933), English translation: The expanding universe, Gen. Rel. Grav. 29, 637 (1997)
- [105] R. C. Tolman, Effect of Inhomogeneity on Cosmological Models, Proc. Natl. Acad. Sci. USA 20, 169-176 (1934)
 - [106] H. Bondi, Spherically Symmetrical Models in General Relativity, Month. Not. Roy. Astr. Soc. 107, 410 (1947)
 - [107] R. K. Sachs, A. M. Wolfe, Perturbations of a Cosmological Model and Angular Variations of the Microwave Background, Astrophysical Journal, vol. 147, p.73 (1967)
 - [108] M. J. Rees, D. W. Sciama, Large-scale Density Inhomogeneities in the Universe, Nature, Volume 217, Issue 5128, pp. 511-516 (1968)
 - [109] Atsushi J. Nishizawa, Integrated Sachs Wolfe Effect and Rees Sciama Effect, Prog. Theor. Exp. Phys. 2014, 06B110
 - [110] P. Szekeres: A class of inhomogeneous cosmological models , Communications in Mathematical Physics 41 (1975), no. 1, 55-64
 - [111] L. Nottale, Perturbation of the Magnitude-Redshift Relation in an Inhomogeneous Relativistic Model: The Redshift Equations, Astron. Astrophys. 110, 9-17 (1982)
 - [112] L. Nottale, Perturbation of the Magnitude-Redshift Relation in an Inhomogeneous Relativistic Model II. Corrections to the Hubble Law Behind Clusters, Astron. Astrophys., 114, 261-269 (1982).
 - [113] L. Nottale, Perturbation of the Magnitude-Redshift Relation in an Inhomogeneous Relativistic Model III. Redshift effect intrinsic to clusters of galaxies, Astron. Astrophys., 118, 85-89 (1983)